

Constraints on a mixed inflaton and curvaton scenario for the generation of the curvature perturbation

George Lazarides,^{1,*} Roberto Ruiz de Austri,^{2,†} and Roberto Trotta^{3,‡}

¹*Physics Division, School of Technology, Aristotle University of Thessaloniki, Thessaloniki 54124, Greece*

²*University of Sheffield, Department of Physics and Astronomy, Hicks Building, Hounsfield Road, Sheffield S3 7RH, England*

³*Département de Physique Théorique, Université de Genève,*

24 quai Ernest Ansermet, 1211 Genève 4, Switzerland

(Dated: November 25, 2018)

We consider a simple supersymmetric grand unified model which naturally solves the strong CP and μ problems via a Peccei-Quinn symmetry and leads to the standard realization of hybrid inflation. We show that the Peccei-Quinn field of this model can act as a curvaton. In contrast to the standard curvaton hypothesis, both the inflaton and the curvaton contribute to the total curvature perturbation. The model predicts the existence of an isocurvature perturbation too which has mixed correlation with the adiabatic one. The cold dark matter of the universe is mostly constituted by axions, which are produced at the QCD phase transition, plus a small amount of lightest sparticles. The predictions of the model are confronted with the first-year Wilkinson microwave anisotropy probe and other cosmic microwave background radiation data. We analyze in detail two representative choices of parameters for our model and derive bounds on the curvaton contribution to the adiabatic perturbation. We find that, for the choice which provides the best fitting of the data, the curvaton contribution to the amplitude of the adiabatic perturbation must be smaller than about 67% and the amplitude of the partial curvature perturbation from the curvaton smaller than 43.2×10^{-5} (both at 95% confidence level). The best-fit power spectra are dominated by the adiabatic part of the inflaton contribution. We use Bayesian model comparison to show that this choice of parameters is disfavored with respect to the pure inflaton scale-invariant case with odds of about 50 to 1. For the second choice of parameters examined, the adiabatic mode is dominated by the curvaton, but this choice is strongly disfavored relative to the pure inflaton scale-invariant case (with odds of about 10^7 to 1). We conclude that in the present framework the perturbations must be dominated by the adiabatic component from the inflaton.

PACS numbers: 12.10.-g, 12.60.Jv, 98.80.Cq

I. INTRODUCTION

Inflation, which was originally proposed [1] as a solution to the outstanding problems of standard big bang cosmology and the problem of unwanted relics, is in good agreement with the recent measurements [2, 3] on the angular power spectrum of the cosmic microwave background radiation (CMBR). Moreover, inflation is now established as the most likely origin of the primordial density perturbation from which structure formation in the universe proceeded [4]. According to the usual assumption [4, 5], this perturbation is generated solely by the slowly rolling inflaton field of the usual one-field inflationary models and, thus, is expected to be purely adiabatic. However, although adiabatic perturbations are perfectly consistent with the present data, the presence of a significant isocurvature density perturbation cannot be excluded [3, 6]. In one-field inflation, the perturbations are almost Gaussian, in agreement with the current upper bounds on non-Gaussianity from the CMBR data,

which though cannot exclude the presence of appreciable non-Gaussianity (for a review, see e.g. Ref. [7]).

Lately, the alternative possibility [8, 9] that the adiabatic density perturbations originate from the inflationary perturbations of some light “curvaton” field different from the inflaton has attracted much attention. The curvaton density perturbations can lead [9, 10], after curvaton decay, to isocurvature perturbations in the densities of the various components of the cosmic fluid. In the simplest case, the residual isocurvature perturbations are either fully correlated or fully anti-correlated with the adiabatic density perturbation. In general models, however, the correlation can be mixed (see e.g. Ref. [11]). In the curvaton scenario, significant non-Gaussianity may also appear. The main reason for advocating the curvaton hypothesis is that it makes [12] the task of constructing viable models of inflation much easier, since it liberates us from the very restrictive requirement that the inflaton is responsible for the curvature perturbations.

In a recent paper [11], a simple extension [13] of the minimal supersymmetric standard model (MSSM) which naturally and simultaneously solves the strong CP and μ problems via a Peccei-Quinn (PQ) [14] and a continuous R symmetry was considered within the general framework of the standard supersymmetric (SUSY) version [15, 16] of hybrid inflation [17]. It was shown that, in this

*Electronic address: lazaride@eng.auth.gr

†Electronic address: r.ruizdeaustri@sheffield.ac.uk

‡Electronic address: roberto.trotta@physics.unige.ch

model, the PQ field, which breaks spontaneously the PQ symmetry, can successfully act as a curvaton generating the total curvature perturbation in the universe in accordance with the cosmic background explorer (COBE) measurements [18]. The (intermediate) PQ scale is generated by invoking supergravity (SUGRA) and the PQ field corresponds to a flat direction in field space lifted by non-renormalizable interactions. Moreover, the μ parameter of MSSM is generated [19] from the PQ scale.

We feel that the standard curvaton hypothesis [8, 9], which insists that the total curvature perturbation originates solely from the curvaton, can also be quite restrictive and not so natural. Indeed, in accordance to this hypothesis, one needs to impose [12] an upper bound on the inflationary scale in order to ensure that the perturbation from the inflaton is negligible. This bound can be quite strong especially if the slow-roll parameter ϵ (see e.g. Ref. [5]) happens to be very small, which holds in many cases. In generic models, one would expect that all the scalar fields which are essentially massless during inflation contribute to the total curvature perturbation. So, in the presence a PQ field, which can be kept [11] light during the relevant part of inflation, it is natural to assume that the adiabatic density perturbation is partly due to this field and partly to the inflaton.

There is yet another reason for abandoning the strict curvaton hypothesis. The recent measurements on the CMBR by the Wilkinson microwave anisotropy probe (WMAP) satellite [2] have considerably strengthened [3, 6, 20] the bound on the isocurvature perturbation which was obtained [21, 22] by using the pre-WMAP CMBR data. As a consequence, the viability of many curvaton models is in doubt. However, allowing a significant part of the total curvature perturbation in the universe to originate from the inflaton, we can hopefully relax the tension between these models and the present WMAP data without losing the main advantage of the curvaton hypothesis, which is that it facilitate the construction of viable inflationary models (see Ref. [23] for recent investigations of this possibility).

The PQ curvaton model of Ref. [11] predicts an isocurvature perturbation of mixed correlation with the curvature perturbation. The extended set of pre-WMAP CMBR and other data which was used [11] to restrict the isocurvature perturbation in the model of Ref. [11] led to the exclusion of a major part of the available parameter space. Including the more restrictive recent WMAP measurements, the allowed parameter space will certainly be further reduced. It is, moreover, quite possible that the model is even totally excluded by these new data. So, the departure from the strict curvaton hypothesis may prove to be vital for this particular curvaton scheme.

In this paper, we will extend the PQ curvaton model of Ref. [11] by embedding it into the concrete SUSY grand unified theory (GUT) model studied in Ref. [24], which is based on the left-right (LR) symmetric gauge group $G_{LR} = SU(3)_c \times SU(2)_L \times SU(2)_R \times U(1)_{B-L}$. This model leads [24] naturally to standard SUSY hybrid in-

flation [15, 16]. After the end of inflation, the inflaton performs damped oscillations about the SUSY vacuum and eventually decays into right handed neutrino superfields reheating the universe. The subsequent decay of these superfields to a lepton and an electroweak Higgs superfield generates [25] a primordial lepton asymmetry [26] which is then partly converted into baryon asymmetry by non-perturbative electroweak sphaleron effects. The observed baryon asymmetry of the universe (BAU) can then be easily reproduced [24] in accord with the data on neutrino masses and mixing. At reheating, gravitinos are also produced thermally. They decay in the late universe leading to lightest sparticles (LSPs), which contribute to the cold dark matter (CDM) in the universe. For simplicity, we assume that this is the only source of relic LSPs neglecting their direct thermal production. Due to the presence of the PQ symmetry, our model contains axions which come into play at the QCD phase transition and can also contribute to CDM.

The PQ field of our model can acquire a super-horizon spectrum of perturbations from inflation provided that it is effectively massless during the relevant part of inflation. It can thus act as curvaton contributing to the total curvature perturbation together with the inflaton. We study the evolution of the PQ field during and after inflation by including corrections [15, 27, 28] to the PQ potential which originate from the SUSY breaking in the early universe caused by the presence of a finite energy density. We assume that these corrections are (somewhat) suppressed, which is [29] indeed the case if specific Kähler potentials are used.

The requirement that the PQ field is essentially massless during inflation yields [11], for given values of the other parameters, an upper bound on the possible values of this field at the end of inflation. Moreover, it implies that, as inflation terminates, the PQ field emerges [11] with negligible velocity. There is also a lower bound on the value of the PQ field at the end of inflation below which the classical equation of motion during inflation for the mean value of this field in a region of fixed size somewhat bigger than the size of the de Sitter horizon ceases [11] to be valid. This is due to the fact that the quantum perturbations of the PQ field from inflation overshadow its classical kinetic energy density. We will exclude this quantum regime since the calculation of the spectral index of the partial curvature perturbation from the curvaton field in this regime is not so clear.

The values of the PQ field at the end of inflation which are not excluded by the above considerations can be classified according to whether they lead to the PQ vacua or the trivial (false) vacuum. We find that, generically, there exist two separate bands of such values leading to the correct (PQ) vacua. One of them lies at relatively low values of the curvaton field at the end of inflation, while the other lies at values which are considerably higher. In all other cases, the system ends up in the wrong (trivial) vacuum and thus the corresponding values of the PQ field at the end of inflation must be excluded. Our numerical

findings show that the (approximate) COBE constraint on the CMBR can be satisfied only within the upper allowed band. This constraint receives contributions not only from the curvature perturbation but also from the isocurvature one and the cross correlation of the two. Note, however, that this constraint is quite approximate and can be considered only as an indicative criterion.

The amplitude and spectral index of the partial curvature perturbation from the inflaton are calculated by employing the analysis of Ref. [5] slightly modified to allow for the possibility that the slow-roll conditions are violated and, thus, hybrid inflation ends before reaching the instability point on the inflationary trajectory. The partial curvature perturbation from the curvaton is treated in a more accurate way than in Ref. [11]. In particular, the evolution during inflation of the perturbation acquired by the PQ field from inflation when our present horizon scale crossed outside the inflationary horizon is considered. It is described by the classical equation of motion for this field in the slow-roll approximation. Solving this equation, we can find the perturbation in the value of the curvaton field at the end of inflation. This same calculation yields the spectral index for the curvaton too. For any given value of the PQ field at the termination of inflation, we take the perturbed value too and follow the subsequent evolution of both these fields until the time of the curvaton decay. This yields the amplitude of the partial curvature perturbation from the curvaton. The total curvature perturbation is then given by the appropriate weighted sum of these two uncorrelated perturbations.

As mentioned already, the baryons and the LSPs in our model originate from reheating. They thus inherit the partial curvature perturbation of the oscillating and decaying inflaton, which is different from the total curvature perturbation due to the presence of the curvaton. As a consequence, the baryons and LSPs acquire an isocurvature perturbation of mixed correlation with the total curvature perturbation. The CDM in our model contains also axions carrying an isocurvature perturbation which is uncorrelated with the perturbations from the inflaton and the curvaton. The amplitude and spectral index of this isocurvature perturbation is evaluated by following the analysis of Ref. [11]. We see that, in our model, the correlation of the total adiabatic and isocurvature perturbations is mixed.

For given values of all the other independent parameters, we take a grid of values of the curvaton field at the end of inflation and the amplitude of partial curvature perturbation from the inflaton which cover the upper or the lower allowed band. We calculate the total CMBR angular power spectrum for each point in this grid. The predictions from each band are confronted with the CMBR temperature (TT) and temperature-polarization (TE) cross correlation angular power spectra from the first-year WMAP observations [2] as well as the CMBR data on smaller scales from the arcminute cosmology bolometer array receiver (ACBAR) [30, 31] and the

cosmic background imager (CBI) [32] experiments. We then study the implications of the resulting restrictions on the various parameters of the model. We also employ Bayesian model testing to compare our model with the standard pure inflaton single-field inflationary model with scale-invariant perturbations. We are particularly interested to see whether the data favor the presence of a non-vanishing curvaton contribution to the adiabatic perturbation.

The paper is organized as follows. In Sec. II, we outline the salient features of our LR SUSY GUT model which solves the strong CP and μ problems via a PQ symmetry and leads to the standard version of SUSY hybrid inflation. The evolution of the PQ field during and after inflation as well as its final decay into light particles are sketched in Sec. III. Section IV is devoted to the evaluation of the total curvature perturbation which, in our case, is partly due to the inflaton and partly to the curvaton. In Sec. V, we estimate the isocurvature perturbations in the relic density of the baryons, the LSPs and the axions. The total CMBR angular power spectrum predicted by our model is discussed in Sec. VI. Our numerical calculation and results are presented and discussed in Sec. VII, and our conclusions are summarized in Sec. VIII. Finally, in the Appendix, we review some useful concepts and results from Bayesian statistics.

II. THE LEFT-RIGHT SUSY GUT MODEL

We will adopt here the SUSY GUT model of Ref. [24] (see also Ref. [33]) which is based on the LR symmetric gauge group G_{LR} . The $SU(2)_L$ doublet left handed quark and lepton superfields are denoted by q_i and l_i respectively, whereas the $SU(2)_R$ doublet antiquark and antilepton superfields by q_i^c and l_i^c respectively ($i=1,2,3$ is the family index). The electroweak Higgs superfield h belongs to a bidoublet $(2, 2)_0$ representation of $SU(2)_L \times SU(2)_R \times U(1)_{B-L}$.

The breaking of G_{LR} to the standard model (SM) gauge group G_{SM} , at a superheavy scale $M \sim 10^{16}$ GeV, is achieved through the superpotential

$$\delta W_1 = \kappa S(l_H^c \bar{l}_H^c - M^2), \quad (1)$$

where l_H^c, \bar{l}_H^c is a conjugate pair of $SU(2)_R$ doublet left handed Higgs superfields with $B - L$ charges equal to 1, -1 respectively, and S is a gauge singlet left handed superfield. The dimensionless coupling constant κ and the mass parameter M can be made real and positive by suitable rephasing of the fields. The SUSY minima of the scalar potential lie on the D-flat direction $l_H^c = \bar{l}_H^{c*}$ at $\langle S \rangle = 0, |\langle l_H^c \rangle| = |\langle \bar{l}_H^c \rangle| = M$.

The model also contains two extra gauge singlet left handed superfields N and \bar{N} for solving [13] the μ problem of MSSM via a PQ symmetry [14], which also solves the strong CP problem. They have the following super-

potential couplings:

$$\delta W_2 = \frac{\lambda N^2 \bar{N}^2}{2m_P} + \frac{\beta N^2 h^2}{2m_P}, \quad (2)$$

where λ and β are dimensionless parameters, which can be made real and positive by an appropriate redefinition of the phases of the superfields and $m_P \simeq 2.44 \times 10^{18}$ GeV is the reduced Planck mass.

In addition to G_{LR} , the model possesses three global U(1) symmetries, namely an anomalous PQ symmetry $U(1)_{PQ}$, a non-anomalous R symmetry $U(1)_R$, and the baryon number symmetry $U(1)_B$. The PQ and R charges of the various superfields are

$$\begin{aligned} PQ: & \quad q^c, l^c, S, l_H^c, \bar{l}_H^c(0), h, \bar{N}(1), q, l, N(-1); \\ R: & \quad h, l_H^c, \bar{l}_H^c, \bar{N}(0), q, q^c, l, l^c, N(1/2), S(1). \end{aligned} \quad (3)$$

Note that global continuous symmetries such as our PQ and R symmetry can effectively arise [34] from the rich discrete symmetry groups encountered in many compactified string theories (see e.g. Ref. [35]).

It is well known that the superpotential in Eq. (1) leads [15, 16] naturally to the standard SUSY realization of hybrid inflation [17]. In particular, the scalar potential which is derived from it possesses a built-in classically flat valley of minima at $l_H^c = \bar{l}_H^c = 0$ and for $|S|$ greater than a critical (instability) value $S_c = M$. This valley can serve as inflationary path. Indeed, the constant tree-level potential energy density $\kappa^2 M^4$ on this path can cause exponential expansion of the universe. Moreover, since this constant energy density breaks SUSY, there are important radiative corrections [16] which provide a logarithmic slope along the inflationary trajectory necessary for driving the system towards the vacua.

It should be noted that the SUSY GUT model considered here does not predict the existence of topological defects such as magnetic monopoles or cosmic strings. In the opposite case, these defects would have been copiously produced [36] at the end of hybrid inflation. The overproduction of magnetic monopoles, in particular, would have led to a cosmological catastrophe and a modification [36, 37] of the standard realization of SUSY hybrid inflation would be needed to avoid this problem. This happens in higher gauge groups such as the Pati-Salam group, which predicts the existence of monopoles carrying two units of Dirac magnetic charge [38]. Cosmic strings, on the other hand, which are generically present in many GUT models [39, 40], would contribute to the cosmological perturbations leading [41] to extra restrictions on the parameters of the model. The reason that our model does not predict cosmic strings is that the G_{LR} breaking is achieved by a conjugate pair of $SU(2)_R$ doublets with $B - L = 1, -1$ which also break the Z_2 subgroup of $U(1)_{B-L}$. This Z_2 , which does not belong to G_{SM} , would have been left unbroken if, alternatively, we had used a pair of $SU(2)_R$ triplets with $B - L = 2, -2$ for this breaking. This would have led to the presence of Z_2 cosmic strings (compare with the Z_2 cosmic strings encountered in the $SO(10)$ GUT model of Ref. [39]).

The part of the tree-level scalar potential which is relevant for the PQ symmetry breaking is derived from the superpotential coupling $\lambda N^2 \bar{N}^2 / 2m_P$ in Eq. (2) and, after soft SUSY breaking mediated by minimal supergravity (SUGRA), is given by [13]

$$V_{PQ} = \frac{1}{2} m_{3/2}^2 \phi^2 \left(1 - \frac{|A| \lambda \phi^2}{8 m_{3/2} m_P} + \frac{\lambda^2 \phi^4}{16 m_{3/2}^2 m_P^2} \right), \quad (4)$$

where $m_{3/2} \sim 1$ TeV is the gravitino mass and A is the dimensionless coefficient of the soft SUSY breaking term corresponding to the superpotential term $\lambda N^2 \bar{N}^2 / 2m_P$. Here, the phases α, φ and $\bar{\varphi}$ of A, N and \bar{N} are taken to satisfy the relation $\alpha + 2\varphi + 2\bar{\varphi} = \pi$ and $|N|, |\bar{N}|$ are assumed equal, which minimizes the potential. Moreover, rotating N on the real axis by an appropriate R transformation, we defined the canonically normalized real scalar PQ field $\phi = 2N$. For $|A| > 4$, this potential has a local minimum at $\phi = 0$ and absolute minima at

$$\langle \phi \rangle^2 \equiv f_a^2 = \frac{2}{3\lambda} \left(|A| + \sqrt{|A|^2 - 12} \right) m_{3/2} m_P \quad (5)$$

with $f_a (> 0)$ being the axion decay constant, i.e. the symmetry breaking scale of $U(1)_{PQ}$. Substituting this vacuum expectation value (VEV) into the superpotential coupling $\beta N^2 h^2 / 2m_P$ in Eq. (2), we obtain a μ term with

$$\mu = \frac{\beta f_a^2}{4m_P} \sim m_{3/2}, \quad (6)$$

as desired [19]. Note that the potential V_{PQ} in Eq. (4) should be shifted [11] by adding to it the constant

$$\begin{aligned} V_0 = & \frac{1}{108\lambda} \left(|A| + \sqrt{|A|^2 - 12} \right) \\ & \times \left[|A| \left(|A| + \sqrt{|A|^2 - 12} \right) - 24 \right] m_{3/2}^3 m_P, \end{aligned} \quad (7)$$

so that it vanishes at its absolute minima.

III. THE PQ FIELD IN THE EARLY UNIVERSE

In the early universe, the PQ potential can acquire sizable corrections from the SUSY breaking caused by the presence of a finite energy density [15, 27, 28]. In particular, during inflation and the subsequent inflaton oscillations, SUSY breaking is transmitted to the PQ system via its coupling to the inflaton given by the SUGRA scalar potential. The resulting corrections, whose scale is set by the Hubble parameter H , dominate over the contributions from hidden sector SUSY breaking as long as $H \gg m_{3/2}$. For simplicity, we will ignore the A term type corrections [28]. To leading order, we then just obtain a correction δm_ϕ^2 to the mass² of the curvaton. For a general Kähler potential, $\delta m_\phi^2 \sim H^2$ with either sign

possible. However, for specific (no-scale like) Kähler potentials, it might be (partially) cancelled [29]. Assuming that $\delta m_\phi^2 > 0$, we write

$$\delta m_\phi^2 = \gamma^2 H^2, \quad (8)$$

where γ can have different values during inflation and inflaton oscillations. Actually, we must assume that, during inflation, $\gamma \ll 1$ so that the PQ field qualifies as an effectively massless field which acquires perturbations from inflation and thus can act as curvaton. Fortunately, the cancellation of δm_ϕ^2 during inflation can, in principle, be “naturally” arranged to be exact (see fourth paper in Ref. [29]). So, for simplicity, we could take $\gamma = 0$ during inflation. On the other hand, large values of γ after the end of inflation would generically lead [42] to a drastic reduction of the density fraction of the PQ field, which thus again would become unable to play the role of curvaton. In view of the fact that, in contrast to the case of inflation, it is not so easy to achieve exact cancellation of δm_ϕ^2 during inflaton oscillations, we will only assume that, after the termination of inflation, γ is somewhat suppressed, say ~ 0.1 (or smaller).

After reheating, the universe is radiation dominated and, thus, $H \simeq 1/2t \leq 1/2t_{\text{reh}} = \Gamma_{\text{infl}}/2$, where t is the cosmic time and $t_{\text{reh}} = \Gamma_{\text{infl}}^{-1}$ the time at reheating with Γ_{infl} being the inflaton decay width. It is easily seen that, in this case, $H \ll m_{3/2}$ as a consequence of the gravitino constraint ($T_{\text{reh}} \lesssim 10^9$ GeV) [43] on the reheat temperature T_{reh} , which is given by [5]

$$T_{\text{reh}} = \left(\frac{45}{2\pi^2 g_*} \right)^{\frac{1}{4}} (\Gamma_{\text{infl}} m_{\text{P}})^{\frac{1}{2}}, \quad (9)$$

where g_* is the effective number of degrees of freedom ($g_* = 228.75$ for the MSSM spectrum). Thus, the SUSY breaking effects from the finite energy density in the universe are subdominant compared to the hidden sector SUSY breaking effects, whose scale is set by $m_{3/2}$.

The PQ potential can acquire temperature corrections too. During the era of inflaton oscillations, they originate from the new radiation [44] which emerges from the decaying inflaton. It has been shown [11], however, that these corrections are overshadowed by the SUGRA ones which, in the latest stages of this era, are, in turn, overshadowed by the terms from hidden sector SUSY breaking. After reheating, the temperature corrections are less important than the ones from the hidden sector as argued in Refs. [37] and [45]. So, the temperature corrections to the PQ potential can be ignored throughout.

We see that, in the early universe, the effective scalar potential for the PQ field can be taken to be

$$V_{\text{PQ}}^{\text{eff}} = V_{\text{PQ}} + \frac{1}{2} \gamma^2 H^2 \phi^2 + V_0. \quad (10)$$

The full effective scalar potential V which is relevant for our analysis here is obtained by adding to $V_{\text{PQ}}^{\text{eff}}$ the potential for standard SUSY hybrid inflation (see e.g. Ref. [5]).

The evolution of the field ϕ is generally governed by the classical equation of motion

$$\ddot{\phi} + 3H\dot{\phi} + V' = 0, \quad (11)$$

where overdots and primes denote derivation with respect to the cosmic time t and the PQ field ϕ respectively. In particular, Eq. (11) describes [46] the evolution during inflation of the mean value of ϕ in a comoving region larger than the inflationary horizon. Actually, this equation starts to be valid a short time after this region crosses outside the de Sitter horizon. The mean value of ϕ , however, in a region of fixed size somewhat bigger than the (almost) constant size of the de Sitter horizon satisfies [47] this equation during inflation provided that it exceeds a certain value ϕ_Q given by

$$V' \sim \frac{3H_{\text{infl}}^3}{2\pi}, \quad (12)$$

where H_{infl} is the almost constant Hubble parameter during inflation. Therefore, if we require that the value ϕ_f (considered positive without loss of generality) which is taken at the end of inflation by the mean ϕ in a region of fixed size somewhat bigger than H_{infl}^{-1} exceeds ϕ_Q , we can be sure [11] that the classical evolution equation holds for this mean field until the end of inflation. For values of the mean ϕ in a region of fixed size somewhat bigger than H_{infl}^{-1} which are smaller than about ϕ_Q , the random walk executed [48] by this mean field due to the quantum perturbations from inflation cannot be neglected and may overshadow [47] its classical motion. Thus, in this case, the classical equation of motion during inflation for this mean ϕ ceases to be valid. For reasons to be discussed later, we will not consider in our analysis values of ϕ_f which lie in the quantum regime, i.e. which are smaller than ϕ_Q (see Secs. IV and VII A). It should be pointed out in passing that the requirement of complete randomization of the mean ϕ in a region of fixed size somewhat bigger than H_{infl}^{-1} as a consequence of its quantum perturbations from inflation implies [49] an even more stringent bound on this mean ϕ given by $V \lesssim H_{\text{infl}}^4$.

Moreover, as explained in the next section, we will have to study only values of ϕ_f for which ϕ is a slowly rolling field during the relevant part of inflation (i.e. during at least the last 50 – 60 e-foldings). It has been shown [11] that, in this case, the PQ field ϕ emerges at the end of inflation with negligible velocity (i.e. derivative with respect to cosmic time). Its subsequent evolution during the matter dominated era of damped inflaton oscillations is given by Eqs. (10) and (11) with $H = 2/3t$. One finds [11] that, depending on the value of ϕ_f , the PQ system eventually enters into a phase of damped oscillations about either the trivial (local) minimum of V_{PQ} at $\phi = 0$ or one of its PQ (absolute) minima at $\phi = \pm f_a$. Of course, values of ϕ_f leading to the trivial minimum must be excluded.

The damped oscillations of the PQ field continue even after reheating, where H becomes equal to $1/2t$. Finally,

this field decays via the second coupling in the superpotential of Eq. (2) into a pair of Higgsinos provided that their mass μ does not exceed half of the mass of the PQ field (see Ref. [11])

$$m_\phi = \frac{m_{3/2}}{\sqrt{3}} (|A|^2 - 12)^{\frac{1}{4}} \left(|A| + (|A|^2 - 12)^{\frac{1}{2}} \right)^{\frac{1}{2}}, \quad (13)$$

which is independent of the parameter λ . The decay time of the PQ field is $t_\phi = \Gamma_\phi^{-1}$, where Γ_ϕ is its decay width, which has been found [11] to be given by

$$\Gamma_\phi = \frac{\beta^2 f_a^2}{8\pi m_{\text{P}}^2} m_\phi. \quad (14)$$

Note that the coherently oscillating PQ field could evaporate [50] as a result of scattering with particles in the thermal bath before it decays into Higgsinos. However, one can show [11] that, in the model under discussion here, this does not happen.

IV. THE CURVATURE PERTURBATION

We will consider here only values of ϕ_f for which the PQ field ϕ is effectively massless, i.e. $V'' \leq H^2$, during (at least) the last 50 – 60 inflationary e-foldings so that it receives a super-horizon spectrum of perturbations from inflation and can act as curvaton. This requirement also guarantees that ϕ is slowly rolling during the relevant part of inflation. The perturbation $\delta\phi$ then evolves at subsequent times and, when ϕ settles into damped quadratic oscillations about the PQ vacua, yields a stable perturbation in the energy density of this field. After the PQ field decays, this perturbation is transferred to radiation, thereby contributing to the total curvature perturbation. On the other hand, the radiation, which originates from the inflaton decay, could carry a curvature perturbation prior to the curvaton decay too. It actually inherits the curvature perturbation of the inflaton. Contrary to the standard curvaton hypothesis [8], we make here the more natural assumption that this perturbation is non-zero and, thus, also contributes to the total curvature perturbation.

The scalar part of the metric perturbation for a flat universe can be written (using the notation of Ref. [51]), in all generality, as follows (for reviews of the gauge invariant theory of cosmological perturbations, see e.g. Ref. [52]):

$$\delta g_{\mu\nu} dx^\mu dx^\nu = -2Adt^2 + 2aB_{,i} dt dx^i + a^2 (2C\delta_{ij} + E_{,ij}) dx^i dx^j, \quad (15)$$

where $\mu, \nu = 0, 1, 2, 3$ and $i, j = 1, 2, 3$. Here, $x^0 = t$ is the physical time, x^i ($i = 1, 2, 3$) are the comoving spatial coordinates, $Y_{,i} \equiv \partial Y / \partial x^i$ ($i = 1, 2, 3$) and δ_{ij} denotes the Kronecker delta. The dimensionless parameter a is the scale factor of the universe, which is normalized to

unity at the present cosmic time. We define the following gauge invariant quantities:

$$\zeta \equiv C - H \frac{\delta\rho}{\rho}, \quad (16)$$

$$\mathcal{R}_{\text{rad}} \equiv -C - H(B - a^2 v), \quad (17)$$

$$\Phi \equiv -C - H(B - a^2 \dot{E}). \quad (18)$$

Here, $\rho = -T_0^0$ is the total energy density in the universe with T_μ^ν being the energy momentum tensor, $\delta\rho = -\delta T_0^0$ is the total density perturbation, and v describes the spatial perturbation in the 4-velocity u^μ of an observer comoving with the total fluid, i.e. $v^i \equiv -\delta u^i / u^0$. The variable ζ represents the curvature perturbation on hypersurfaces of uniform density, \mathcal{R}_{rad} is the curvature perturbation in the (total matter) comoving gauge (up to the sign), while Φ is the Bardeen potential, which is the curvature perturbation (up to the sign) in the longitudinal gauge. These three quantities are related by

$$\zeta = -\mathcal{R}_{\text{rad}} - \frac{2\rho}{9(\rho + p)} \left(\frac{k}{Ha} \right)^2 \Phi, \quad (19)$$

where we have used the time-time component of the Einstein equation and p is the total pressure of the universe (i.e. $T_{ij} = p\delta_{ij}$). On super-horizon scales, $k \ll Ha$, the second term on the right hand side of this equation is negligible, and we thus have $\zeta = -\mathcal{R}_{\text{rad}}$.

Using Eq. (16), the total curvature perturbation [53] in the flat slicing gauge (defined by setting $C = E = 0$ in Eq. (15)) is given by

$$\zeta = \frac{\delta\rho}{3(\rho + p)}. \quad (20)$$

After the curvaton decay, it becomes [10]

$$\zeta = (1 - f)\zeta_i + f\zeta_c, \quad (21)$$

where $\zeta_i = \delta\rho_r / 4\rho_r$ and $\zeta_c = \delta\rho_\phi / 3\rho_\phi$ are the partial curvature perturbations on spatial hypersurfaces of constant curvature from the inflaton and the curvaton respectively at the curvaton decay with ρ_r and ρ_ϕ being the radiation and ϕ energy densities respectively, and $\delta\rho_r$ and $\delta\rho_\phi$ the corresponding perturbations. Also,

$$f = \frac{3\rho_\phi}{3\rho_\phi + 4\rho_r} \quad (22)$$

evaluated at the time of the curvaton decay. Here, we assume that the amplitude of the oscillating ϕ has been sufficiently reduced so that the potential can be approximately considered as quadratic. Actually, as shown in Ref. [42], this must necessarily happen before the curvaton decays. The oscillating curvaton field then behaves like pressureless matter and $\zeta_c = 2\delta\phi_0 / 3\phi_0$, where ϕ_0 is the amplitude of the oscillations and $\delta\phi_0$ the perturbation in this amplitude originating from the perturbation $\delta\phi_f$ in the value ϕ_f of ϕ at the end of inflation.

The comoving curvature perturbation \mathcal{R}_{rad} , for super-horizon scales, is given by

$$\mathcal{R}_{\text{rad}} = (1-f)A_i \left(\frac{k}{H_0}\right)^{\nu_i} \hat{a}_i + fA_c \left(\frac{k}{H_0}\right)^{\nu_c} \hat{a}_c, \quad (23)$$

where k is the comoving (present physical) wave number, H_0 is the present value of the Hubble parameter and \hat{a}_i, \hat{a}_c are independent normalized Gaussian random variables. Also, A_i and A_c are, respectively, the amplitudes of $-\zeta_i$ and $-\zeta_c$ at the present horizon scale (i.e. at $k = H_0$), and ν_i and ν_c are the spectral tilts of the inflaton and curvaton respectively, which are related to the corresponding spectral indices n_i and n_c by $n_i = 1 + 2\nu_i$ and $n_c = 1 + 2\nu_c$. We do not consider running of the spectral indices, since this is negligible in our model.

The amplitude A_i of the partial curvature perturbation from the inflaton is found [24] to be

$$A_i = \left(\frac{2N_Q}{3}\right)^{\frac{1}{2}} \left(\frac{M}{m_{\text{P}}}\right)^2 x_Q^{-1} y_Q^{-1} \Lambda(x_Q^2)^{-1} \quad (24)$$

with

$$\Lambda(z) = (z+1)\ln(1+z^{-1}) + (z-1)\ln(1-z^{-1}), \quad (25)$$

$$y_Q^2 = \int_{x_f^2}^{x_Q^2} \frac{dz}{z} \Lambda(z)^{-1}, \quad y_Q \geq 0. \quad (26)$$

Here, N_Q is the number of e-foldings suffered by our present horizon scale during inflation, $x_Q = S_Q/M$ with S_Q being the value of $|S|$ when our present horizon scale crosses outside the inflationary horizon, and $x_f = S_f/M$ with S_f being the value of $|S|$ at the end of inflation.

In our model, the slow-roll parameters for the inflaton as functions of $|S|$ are given by [5]

$$\epsilon_i = \left(\frac{\kappa^2 m_{\text{P}}}{8\pi^2 M}\right)^2 z \Lambda(z)^2, \quad (27)$$

$$\eta_i = 2 \left(\frac{\kappa m_{\text{P}}}{4\pi M}\right)^2 \left[(3z+1)\ln(1+z^{-1}) + (3z-1)\ln(1-z^{-1}) \right], \quad (28)$$

where $z = x^2$ with $x = |S|/M$. In the presence of the curvaton, however, one can show that the slow-roll conditions (for $\gamma \rightarrow 0$) take the form $\epsilon, |\eta_i| \leq 1$, where

$$\epsilon \equiv -\frac{\dot{H}}{H^2} = \epsilon_i + \epsilon_c \quad (29)$$

with

$$\epsilon_c = \frac{1}{2} m_{\text{P}}^2 \left(\frac{V'}{V}\right)^2, \quad (30)$$

and x_f is given by the value of x for which these conditions are saturated. Actually, as it turns out, x_f corresponds to $\eta_i = -1$. For $\kappa \ll 1$, the slow-roll conditions are violated only extremely close to the critical point at $x = 1$ ($|S| = S_c$). So, inflation continues practically until this point is reached and, following Ref. [24], we can put $x_f = 1$ in Eq. (26). However, for larger values of the parameter κ , inflation can terminate well before reaching the instability point.

Finally, κ, N_Q are given by [5]

$$\kappa = \frac{2\pi}{\sqrt{N_Q}} y_Q \frac{M}{m_{\text{P}}}, \quad (31)$$

$$N_Q \simeq 55.9 + \frac{2}{3} \ln \frac{\kappa^{\frac{1}{2}} M}{10^{15} \text{ GeV}} + \frac{1}{3} \ln \frac{T_{\text{reh}}}{10^9 \text{ GeV}} \quad (32)$$

(for $H_0 \simeq 72 \text{ km sec}^{-1} \text{ Mpc}^{-1}$). The spectral index for the inflaton is $n_i = 1 - 6\epsilon + 2\eta_i$ (for $\gamma \rightarrow 0$), where ϵ and η_i are evaluated at the time when our present horizon scale crosses outside the inflationary horizon. Note that ϵ enters in this formula, not ϵ_i as in the case of pure inflaton. However, ϵ_c is normally much smaller than ϵ_i which, in turn, is negligible compared to $|\eta_i|$. As a consequence, $n_i \simeq 1 + 2\eta_i$.

We now calculate the amplitude A_c of the partial curvature perturbation from the curvaton ϕ . This originates from the perturbation $\delta\phi_* = (H_*/2\pi)\hat{a}_c$ acquired by ϕ from inflation when our present horizon scale crosses outside the de Sitter horizon (H_* is the inflationary Hubble parameter at that moment). In order to find the evolution of this perturbation during the subsequent part of inflation and estimate its value $\delta\phi_f$ at the end of inflation, we must consider the equation of motion for ϕ during inflation (see Eq. (11)). In the slow-roll approximation, which is assumed to hold for the curvaton too, this equation reads

$$3H\dot{\phi} + V' = 0. \quad (33)$$

Taking a small perturbation $\delta\phi$ of ϕ , Eq. (33) gives

$$3H\delta\dot{\phi} + 3H'\delta\phi\dot{\phi} + V''\delta\phi = 0. \quad (34)$$

Substituting $\dot{\phi}$ from Eq. (33) and using the Friedmann equation $3H^2 m_{\text{P}}^2 = V$, Eq. (34) becomes

$$\delta\dot{\phi} + H(-\epsilon_c + \eta_c)\delta\phi = 0, \quad (35)$$

where

$$\eta_c = m_{\text{P}}^2 \frac{V''}{V}. \quad (36)$$

Integration of Eq. (35) from the cosmic time t_* when our present horizon scale crossed outside the inflationary horizon until the end of inflation (at time t_f) yields

$$\delta\phi_f = \frac{H_*}{2\pi} \hat{a}_c \exp \int_0^{N_Q} (\epsilon_c - \eta_c) dN, \quad (37)$$

where we used the relation $dN = -Hdt$ for the number of e-foldings $N(k) = N_Q + \ln(H_0/k)$ suffered by the scale which corresponds to the comoving wave number k during hybrid inflation.

For each value $\phi_f (> 0)$ of the curvaton field at the end of inflation, we construct the perturbed field $\phi_f + \delta\phi_f$. We then follow the evolution of ϕ_f and $\phi_f + \delta\phi_f$ until the time t_ϕ of the curvaton decay and evaluate the value of $\delta\rho_\phi/\rho_\phi$ at this time. The amplitude A_c of the partial curvature perturbation from the curvaton is given by

$$A_c \hat{a}_c = \frac{1}{3} \frac{\delta\rho_\phi}{\rho_\phi}. \quad (38)$$

We have found numerically that the perturbation $\delta\phi_0$ in the amplitude of the oscillating curvaton at t_ϕ is proportional to $\delta\phi_f$. So ζ_c has the same spectral tilt as $\delta\phi_f$, which can be found from Eq. (37):

$$\nu_c \equiv \frac{d \ln A_c}{d \ln k} = -\epsilon - \epsilon_c + \eta_c, \quad (39)$$

where we used the relation $d \ln k = Hdt$, and ϵ , ϵ_c and η_c are evaluated at t_* . (Note that a similar formula has been derived in the first paper in Ref. [9], but without the $-\epsilon_c$ term in the right hand side.) The spectral index for the curvaton is then $n_c = 1 - 2\epsilon - 2\epsilon_c + 2\eta_c$ which, in most cases, reduces to $n_c \simeq 1 + 2\eta_c$ since we typically have $\epsilon_i, \epsilon_c \ll |\eta_c|$.

It should be pointed out that, in deriving Eq. (39), we assume that, during inflation, the mean value of ϕ in any region of fixed size (somewhat bigger than) H_{infl}^{-1} is initially the same and follows the classical equation of motion (Eq. (11)). This mean field sets the (initial) value of the mean ϕ in any comoving region at the time this region exits the de Sitter horizon. Thus, if it satisfies the above requirements, we can be sure that, at any given time during inflation, the resulting mean ϕ in each comoving region that already exited the horizon is practically independent from the size of this region. So the mean ϕ in a fixed region of size H_{infl}^{-1} or in any comoving volume (after horizon exit) is described by the same (single-valued) function of the cosmic time and evolves classically (in fact, it rolls down slowly in our case). The derivation with respect to time of the logarithm of the amplitude of $\delta\phi_f$, which is given by Eq. (37), is then straightforward leading to Eq. (39). On the contrary, if the mean field in a fixed region of size somewhat bigger than H_{infl}^{-1} executes a random walk with step of amplitude $H_{\text{infl}}/2\pi$ per Hubble time, the calculation of the spectral tilt becomes less clear. So, we decided to exclude the quantum regime (i.e. the region $\phi_f < \phi_Q$) from our analysis (see Sec. VII A). It is true, however, that it is by no means necessary to avoid the random walk behavior at all times during inflation. Indeed, only cosmological scales corresponding to a few e-foldings after the exit of our present horizon scale from the de Sitter horizon are relevant. For simplicity though, we exclude all the quantum regime so that no random motion of the mean ϕ in a region of size H_{infl}^{-1} is encountered during inflation. This, as we will see, has no influence on our results.

V. THE ISOCURVATURE PERTURBATION

After the termination of inflation, the inflaton performs damped oscillations about the SUSY vacuum and eventually decays into light particles reheating the universe. At reheating, gravitinos are thermally produced besides other particles. They only decay, though, well after the big bang nucleosynthesis (BBN) since they have very weak couplings. Each decaying gravitino yields one sparticle subsequently turning into the LSP, which is stable. These LSPs survive until the present time contributing to the relic abundance of CDM in the universe. For simplicity, we assume that the thermally produced LSPs can be neglected, which holds in many cases. So, all the relic LSPs come solely from the decaying gravitinos. Baryons can be produced via a primordial leptogenesis [26] which can occur [25] at reheating.

We see that both the LSPs and the baryons originate from reheating. Their partial curvature perturbations, ζ_{LSP} and ζ_B respectively, should thus coincide with the partial curvature perturbation of the radiation which emerges from the inflaton decay, i.e.

$$\zeta_{\text{LSP}} = \zeta_B = \zeta_i. \quad (40)$$

The isocurvature perturbation of the LSPs and the baryons is then given by

$$\mathcal{S}_{\text{LSP+B}} \equiv 3(\zeta_{\text{LSP+B}} - \zeta) = 3f(\zeta_i - \zeta_c), \quad (41)$$

where $\zeta_{\text{LSP+B}} = \zeta_{\text{LSP}} = \zeta_B$ is the partial curvature perturbation of the LSPs and the baryons and we used Eq. (21). Here, we assume that the curvature perturbation in radiation (ζ_γ) practically coincides with the total curvature perturbation. This corresponds to a negligible neutrino isocurvature perturbation, which is [10] the case provided that, as in our model, leptogenesis takes place well before the curvaton decays or dominates the energy density. Applying the definitions which follow Eq. (23), Eq. (41) takes the form

$$\mathcal{S}_{\text{LSP+B}} = -3fA_i \left(\frac{k}{H_0}\right)^{\nu_i} \hat{a}_i + 3fA_c \left(\frac{k}{H_0}\right)^{\nu_c} \hat{a}_c. \quad (42)$$

Our model contains axions which can also contribute to the CDM of the universe. They are produced at the QCD phase transition, which occurs well after the curvaton decay. They carry an isocurvature perturbation, which is completely uncorrelated with the curvature perturbation and can be written as

$$\mathcal{S}_a = A_a \left(\frac{k}{H_0}\right)^{\nu_a} \hat{a}_a, \quad (43)$$

where A_a is its amplitude at the present horizon scale, ν_a is the corresponding spectral tilt (yielding the spectral index $n_a = 1 + 2\nu_a$) and \hat{a}_a is a normalized Gaussian random variable which is independent from \hat{a}_i and \hat{a}_c .

The amplitude A_a is given by [11]

$$A_a = \frac{H_*}{\pi|\theta|\phi_*}, \quad (44)$$

where θ is the so-called initial misalignment angle, i.e. the phase of the complex PQ field during (and at the end of) inflation and ϕ_* is the value of ϕ at t_* . In our case, the angle θ lies [11] in the interval $[-\pi/6, \pi/6]$ with all values in it being equally probable. It is determined by considering the total CDM abundance $\Omega_{\text{CDM}}h^2$ which, in our model, is the sum of the relic abundance [54]

$$\Omega_{\text{LSP}}h^2 \simeq 0.0074 \left(\frac{m_{\text{LSP}}}{200 \text{ GeV}} \right) \left(\frac{T_{\text{reh}}}{10^9 \text{ GeV}} \right) \quad (45)$$

of the LSPs coming from the gravitino decays and the relic axion abundance [55]

$$\Omega_a h^2 \simeq \theta^2 \left(\frac{f_a}{10^{12} \text{ GeV}} \right)^{1.175}. \quad (46)$$

Here $\Omega_j = \rho_j/\rho_c$ with ρ_j being the present energy density of the j th species and ρ_c the present critical energy density of the universe. Furthermore, m_{LSP} is the LSP mass and $H_0 = 100h \text{ km sec}^{-1} \text{ Mpc}^{-1}$ the present Hubble parameter. In the numerical calculation of M and the amplitudes A_c and A_a for given A_i and ϕ_f (see Secs. VII A and VII B), we will fix $h \simeq 0.72$, which is its best-fit value from the Hubble space telescope (HST) [56]. (In the full Monte Carlo (MC) CMBR analysis, however, we do allow h to vary as detailed in Sec. VII D 1.) This approximation has very little influence on the accuracy of the results (see the remarks at the end of Sec. VII B). Note that, in deriving the estimate for $\Omega_a h^2$ in Eq. (46), we applied the simplifying assumptions of Ref. [11].

The spectral tilt ν_a is evaluated by observing that the potential of the axion field remains flat until the QCD transition is reached. So, there is no evolution of θ and its perturbation $\delta\theta = (H_*/2\pi\phi_*)\hat{a}_a$ after crossing outside the inflationary horizon and until the onset of axion oscillations. The axion isocurvature perturbation, which is [11] equal to $2\delta\theta/\theta$, depends on the scale only through H_*/ϕ_* . We find

$$\nu_a = -\epsilon + \frac{m_{\text{P}}}{\phi_*} \frac{V'}{V} m_{\text{P}} = -\epsilon + \frac{m_{\text{P}}}{\phi_*} \sqrt{2\epsilon_c}, \quad (47)$$

where Eqs. (30) and (33) were used, and the slow-roll parameters ϵ and ϵ_c are evaluated at t_* . In view of the fact that ϵ is normally negligible, Eq. (47) reduces to $\nu_a \simeq m_{\text{P}}\sqrt{2\epsilon_c}/\phi_*$ and $n_a \simeq 1 + 2m_{\text{P}}\sqrt{2\epsilon_c}/\phi_*$.

Combining Eqs. (42) and (43), we find that the total isocurvature perturbation is [11]

$$\mathcal{S}_{\text{rad}} = \frac{\Omega_{\text{LSP}+B}}{\Omega_m} \mathcal{S}_{\text{LSP}+B} + \frac{\Omega_a}{\Omega_m} \mathcal{S}_a, \quad (48)$$

where we used the definitions $\Omega_{\text{LSP}+B} \equiv \Omega_{\text{LSP}} + \Omega_B$ and $\Omega_m \equiv \rho_m/\rho_c = \Omega_{\text{LSP}+B} + \Omega_a$ with ρ_m being the total matter density at present.

VI. THE CMBR POWER SPECTRUM

In order to calculate the expected total CMBR angular power spectrum C_ℓ in our model, we must first

specify the various contributions to the amplitude of the total adiabatic and isocurvature perturbation as well as the cross correlation between these two perturbations. In the following, all the amplitudes are referred to the pivot scale k_{P} , for which we use the customary value $k_{\text{P}} = 0.05 \text{ Mpc}^{-1}$ [57]. We thus define the amplitudes of the partial curvature perturbations from the inflaton ($A_{\text{P},i}$) and the curvaton ($A_{\text{P},c}$), and the amplitude of the isocurvature perturbation in the axions ($A_{\text{P},a}$) at $k = k_{\text{P}}$:

$$A_{\text{P},i} = A_i \left(\frac{k_{\text{P}}}{H_0} \right)^{\nu_i}, \quad A_{\text{P},c} = A_c \left(\frac{k_{\text{P}}}{H_0} \right)^{\nu_c},$$

$$A_{\text{P},a} = A_a \left(\frac{k_{\text{P}}}{H_0} \right)^{\nu_a}, \quad (49)$$

where the amplitudes A_i , A_c and A_a at $k = H_0$ are given in Eqs. (24), (38) and (44) respectively.

From Eq. (23), we find that the amplitude squared of the adiabatic perturbation at the pivot scale is given by

$$R^2 = \langle \mathcal{R}_{\text{rad}} \mathcal{R}_{\text{rad}} \rangle = R_i^2 + R_c^2, \quad (50)$$

where \mathcal{R}_{rad} is evaluated at $k = k_{\text{P}}$, and the inflaton (R_i^2) and curvaton (R_c^2) contributions to this amplitude squared are

$$R_i^2 = (1-f)^2 A_{\text{P},i}^2 \quad \text{and} \quad R_c^2 = f^2 A_{\text{P},c}^2. \quad (51)$$

The curvaton fractional contribution to the amplitude of the adiabatic perturbation is defined as follows:

$$F_c^{\text{rad}} = \frac{R_c}{R}. \quad (52)$$

The amplitude squared of the isocurvature perturbation at k_{P} is found from Eq. (48) to be

$$S^2 = \langle \mathcal{S}_{\text{rad}} \mathcal{S}_{\text{rad}} \rangle = S_i^2 + S_c^2 + S_a^2, \quad (53)$$

where

$$S_i^2 = 9f^2 \left(\frac{\Omega_{\text{LSP}+B}}{\Omega_m} \right)^2 A_{\text{P},i}^2,$$

$$S_c^2 = 9f^2 \left(\frac{\Omega_{\text{LSP}+B}}{\Omega_m} \right)^2 A_{\text{P},c}^2 \quad \text{and} \quad S_a^2 = \left(\frac{\Omega_a}{\Omega_m} \right)^2 A_{\text{P},a}^2 \quad (54)$$

are, respectively, the inflaton, curvaton and axion contributions to this amplitude squared.

The cross correlation between the adiabatic and isocurvature perturbation at the pivot scale k_{P} is

$$C = \langle \mathcal{R}_{\text{rad}} \mathcal{S}_{\text{rad}} \rangle = C_i + C_c, \quad (55)$$

where

$$C_i = -R_i S_i \quad \text{and} \quad C_c = R_c S_c \quad (56)$$

are the contributions from the inflaton and the curvaton respectively. Observe that the axions do not contribute to the cross correlation (and the amplitude of the adiabatic perturbation). Also, note that the isocurvature perturbation from the inflaton is fully anti-correlated with the corresponding adiabatic perturbation, whereas the isocurvature perturbation from the curvaton is fully correlated with the adiabatic perturbation from it. So the overall correlation is mixed. It is thus useful to define [22] the dimensionless cross correlation $\cos \Delta$ as a measure of the correlation between adiabatic and isocurvature perturbations and the entropy-to-adiabatic ratio B at k_P :

$$\cos \Delta = \frac{C}{RS} \quad \text{and} \quad B = \frac{S}{R}. \quad (57)$$

The total CMBR angular power spectrum is given, in the notation of Ref. [51], by the superposition

$$C_\ell = C_\ell^{\text{ad}} + C_\ell^{\text{is}} + C_\ell^{\text{cc}}, \quad (58)$$

where

$$C_\ell^{\text{ad}} = R_i^2 C_\ell^{\text{ad},n_i} + R_c^2 C_\ell^{\text{ad},n_c}, \quad (59)$$

$$C_\ell^{\text{is}} = S_i^2 C_\ell^{\text{is},n_i} + S_c^2 C_\ell^{\text{is},n_c} + S_a^2 C_\ell^{\text{is},n_a}, \quad (60)$$

$$C_\ell^{\text{cc}} = C_i C_\ell^{\text{cc},n_i} + C_c C_\ell^{\text{cc},n_c}. \quad (61)$$

The above relations hold for the TT, E-polarization (EE) and TE cross correlation angular power spectra.

The TT power spectrum on large angular scales (i.e. for $\ell \lesssim 20$), can be approximated by (see e.g. Ref. [51])

$$\begin{aligned} C_\ell^{\text{TT}} = & \frac{2\pi^2}{25} [(R_i^2 + 4S_i^2 - 4C_i)f(n_i, \ell) \\ & + (R_c^2 + 4S_c^2 - 4C_c)f(n_c, \ell) \\ & + 4S_a^2 f(n_a, \ell)], \end{aligned} \quad (62)$$

where

$$f(n, \ell) = (\eta_0 k_P)^{1-n} \frac{\Gamma(3-n)\Gamma(\ell - \frac{1}{2} + \frac{n}{2})}{2^{3-n}\Gamma^2(2 - \frac{n}{2})\Gamma(\ell + \frac{5}{2} - \frac{n}{2})} \quad (63)$$

with $\eta_0 = 2H_0^{-1} \simeq 8.33 \times 10^3$ Mpc being the value of conformal time in the present (matter dominated) universe. The derivation of Eq. (62) assumes that the universe is completely matter dominated at the moment of recombination, and further neglects the late integrated Sachs-Wolfe (ISW) effect from the cosmological constant. Therefore this expression is accurate to about 10 – 20% and gives an order of magnitude estimate only. For scale-invariant spectra, $f(n = 1, \ell) = 1/\pi\ell(\ell + 1)$ and the Sachs-Wolfe (SW) plateau is flat. Notice from Eq. (62) that a positively correlated perturbation (as the perturbation from the curvaton) displays less power on large

angular scales, because the cross correlation term subtracts power and can partially cancel the isocurvature contribution. On the contrary, a negatively correlated perturbation (such as the one from the inflaton) presents larger power on the COBE scales and, therefore, can be more easily constrained. The COBE measurements give [58] the following central value for $\ell = 10$:

$$\ell(\ell + 1)C_\ell^{\text{TT}}/2\pi|_{\ell=10} \approx 1.05 \times 10^{-10}. \quad (64)$$

We will apply this COBE constraint with C_ℓ^{TT} evaluated from Eq. (62) only as an indicative (approximate) criterion to get a first rough feeling on the possible compatibility of our model with the data.

VII. NUMERICAL CALCULATIONS AND RESULTS

A. The cosmological evolution of ϕ

We are now ready to proceed to the numerical study of the evolution of the PQ field during and after inflation. To this end, we fix the parameter κ in the superpotential δW_1 in Eq. (1) for standard hybrid inflation. Then, for any given value of the amplitude A_i of the partial curvature perturbation from the inflaton, we solve Eqs. (24), (31) and (32), where x_f is the solution of $\eta_i = -1$ with η_i given by Eq. (28) and T_{reh} , which enters Eq. (32), is taken equal to 10^9 GeV by saturating the gravitino bound [43]. We thus determine the mass parameter M , which is the magnitude of the VEV breaking the G_{LR} symmetry. Subsequently, we find the (almost constant) inflationary Hubble parameter $H_{\text{infl}} = \kappa M^2/\sqrt{3}m_P$. The parameters M and H_{infl} as functions of the amplitude A_i are shown in Figs. 1 and 2 respectively for $\kappa = 3 \times 10^{-3}$ (solid line) or 3×10^{-2} (dashed line). Note that much smaller values of κ would be considered unnatural. On the other hand, much bigger κ 's would push inflation to higher values of the inflaton field, where SUGRA corrections become important and may ruin [15] inflation.

For any given A_i , we chose a value ϕ_f of ϕ at the end of inflation, which takes place at cosmic time $t_f = 2/3H_{\text{infl}}$. We then solve the classical equation of motion for ϕ during inflation in the slow-roll approximation going backwards in time ($t \leq t_f$) by taking $m_{3/2} = 300$ GeV (which is [59] approximately its minimal value in the constrained MSSM with Yukawa unification [60]), $|A| = 5$ and a fixed value for λ ($\sim 10^{-4}$) in the PQ potential. Note that much bigger values of $|A|$ (recall that $|A| > 4$) or much smaller values of λ would not only be unnatural, but also would lead to an enhancement of the axion decay constant f_a (see Eq. (5)) and thus require unnaturally small misalignment angles θ to achieve the observed total CDM abundance (see Eq. (46)). On the other hand, much bigger values of λ would reduce f_a leading to an unacceptably small CDM abundance. Finally, the parameter γ during inflation is put equal to zero for simplicity (see Sec. III).

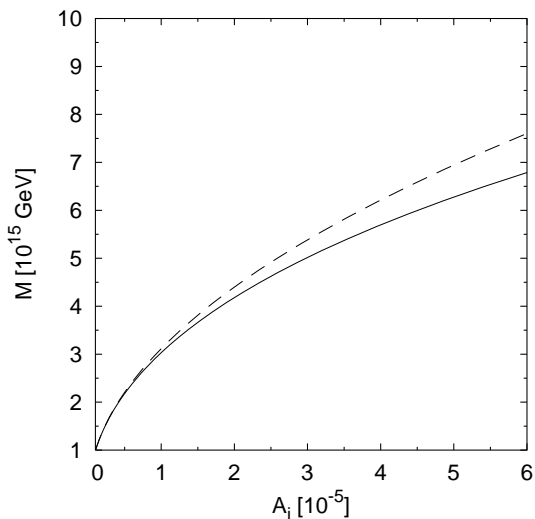


FIG. 1: The mass parameter M versus A_i for $\kappa = 3 \times 10^{-3}$ (solid line) or 3×10^{-2} (dashed line).

We find that, as we move backwards in time, the value of ϕ increases and becomes infinite at a certain moment. Also, the number of e-foldings elapsed from this moment of time until the end of inflation is finite providing an upper bound N_{\max} on the number of e-foldings which is compatible with our boundary condition $\phi = \phi_f$ at t_f .

In order to get a (rough) understanding of this behavior, we approximate the derivative of the potential V with respect to ϕ by $V' \simeq 3\lambda^2\phi^5/16m_{\text{P}}^2$, which holds for $\phi \rightarrow \infty$. The slow-roll equation for ϕ during inflation can then be solved analytically and yields

$$\phi \simeq \frac{\phi_f}{\left(1 + \frac{\lambda^2\phi_f^4}{4m_{\text{P}}^2 H_{\text{infl}}^2} \Delta t\right)^{\frac{1}{4}}}, \quad (65)$$

where $\Delta t = t - t_f \leq 0$. It is obvious from this equation that, as $\Delta t \rightarrow \Delta t_{\min} \equiv -4m_{\text{P}}^2 H_{\text{infl}}/\lambda^2\phi_f^4$, $\phi \rightarrow \infty$. This implies that the maximal number of e-foldings which is allowed for a given value of ϕ_f is $N_{\max} \simeq -H_{\text{infl}}\Delta t_{\min} = 4m_{\text{P}}^2 H_{\text{infl}}^2/\lambda^2\phi_f^4$. Needless to say that no approximation for V' is used when we actually calculate N_{\max} .

It is clear that we must first impose the requirement that $N_{\max} \geq N_Q$. The time t_* at which our present horizon scale crosses outside the inflationary horizon can then be determined from $N_Q = H_{\text{infl}}(t_f - t_*)$. Furthermore, we demand that, at t_* , $V'' \leq H_{\text{infl}}^2$, which ensures that this inequality holds for all times between t_* and t_f . This condition, thus, guarantees that the PQ field is effectively massless during the relevant part of inflation and can act as curvaton. It also provides us with an *a posteriori* justification of the validity of the slow-roll approximation used and ensures that the velocity of ϕ at the end of inflation is negligible. This masslessness requirement yields an upper bound on ϕ_f for every given A_i and fixed values of κ and λ . The excluded region in the $A_i - \phi_f$ plane for fixed κ and λ is represented as a

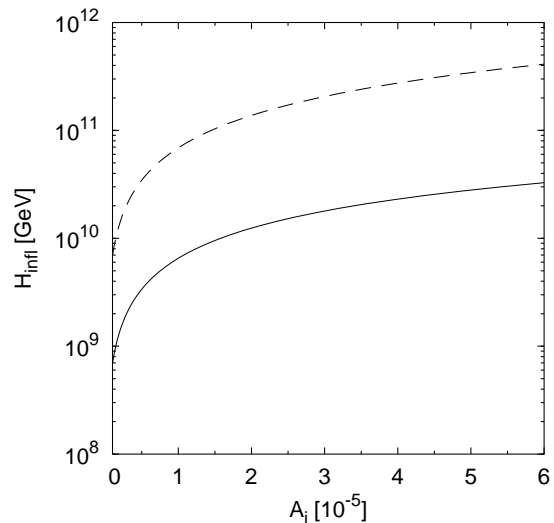


FIG. 2: The inflationary Hubble parameter H_{infl} versus A_i for $\kappa = 3 \times 10^{-3}$ (solid line) or 3×10^{-2} (dashed line).

red/dark shaded area in the upper part of this plane. In Figs. 3 and 4, we show this upper red/dark shaded area for $\kappa = 3 \times 10^{-3}$, $\lambda = 10^{-4}$ (model A) and $\kappa = 3 \times 10^{-2}$, $\lambda = 10^{-4}$ (model B) respectively. The lower red/dark shaded area in the $A_i - \phi_f$ plane corresponds to the quantum regime and is also excluded for the reasons explained at the end of Sec. IV (see Figs. 3 and 4). This also ensures that, at any given instant of time during inflation, ϕ has practically the same mean value in all comoving volumes (which crossed outside the horizon). So, during inflation, ϕ can be simply considered as a function of time only.

We start from any given value of ϕ_f at t_f which is not excluded by the above considerations and assume vanishing time derivative of ϕ at t_f . As explained above, this is a good approximation provided that ϕ_f does not belong to the upper red/dark shaded area in the $A_i - \phi_f$ plane (see Figs. 3 and 4). Moreover, we find numerically that the subsequent evolution of ϕ remains practically unchanged if we take a small non-vanishing value of ϕ at t_f . Under these initial conditions at t_f , we follow the evolution of the field at subsequent times ($t \geq t_f$) by solving the classical equation of motion in Eq. (11) with $H = 2/(3t)$ for $t_f \leq t \leq t_{\text{reh}}$ and $H = 1/(2(t - t_{\text{reh}}/4))$ for $t_{\text{reh}} \leq t \leq t_\phi$. In the latter expression for H , we subtracted $t_{\text{reh}}/4$ from t in order to achieve continuity of H at $t = t_{\text{reh}}$. The time of reheating t_{reh} is calculated by using Eq. (9) with $g_* = 228.75$ and the curvaton decay time t_ϕ is found by employing Eq. (14) with β from Eq. (6), where μ is taken equal to 300 GeV, which is smaller than half the curvaton mass (see Eq. (13)) so that the decay of ϕ to Higgsinos is not blocked kinematically. The parameter γ in the effective PQ potential of Eq. (10) is taken equal to 0.1 after the end of inflation (see Sec. III). We find that, for fixed κ and λ , there exist two bands in the $A_i - \phi_f$ plane which lead to the desired PQ vacua at t_ϕ . They are depicted as an upper and a lower green/lightly

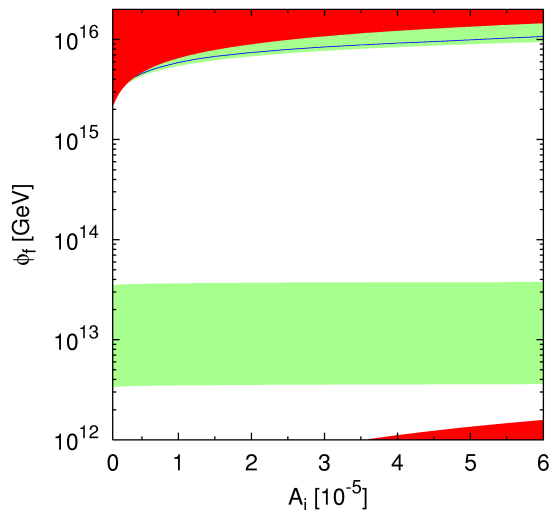


FIG. 3: The two green/lightly shaded bands in the $A_i - \phi_f$ plane which lead to the PQ vacua at t_ϕ for $\kappa = 3 \times 10^{-3}$, $\lambda = 10^{-4}$ (model A). The white (not shaded) areas lead to the trivial vacuum and are thus excluded. The upper red/dark shaded area is excluded by the requirement that, at t_* , $V'' \leq H_{\text{infl}}^2$, while the lower one corresponds to the quantum regime. The blue/solid line shows the values of A_i , ϕ_f which approximately reproduce the correct value of the CMBR large scale temperature anisotropy, as measured by COBE (see Sec. VIIC for details).

shaded band (see Figs. 3 and 4). The white (not shaded) areas in the $A_i - \phi_f$ plane lead to the false (trivial) minimum at $\phi = 0$ and thus must be excluded. Note that, for all relevant κ 's and λ 's, the quantum regime overlaps (at most) with the lower green/lightly shaded band only. However, as we will see later, this band is anyway excluded by the data in all cases, the reason being that it predicts an unacceptably large isocurvature perturbation. So, the *a priori* exclusion of the quantum regime does not affect our results in any essential way.

Besides models A and B (we summarize the corresponding parameter values in Table I), which will be used as our main examples in this presentation, we have also studied three extra pairs of values of κ and λ , namely $\kappa = 10^{-3}$ and $\lambda = 10^{-4}$, $\kappa = 10^{-2}$ and $\lambda = 10^{-4}$, and $\kappa = 3 \times 10^{-2}$ and $\lambda = 3 \times 10^{-4}$ (see below). In the first two cases, the behavior was found to be quite close to the behavior of model A as depicted in Fig. 3, while the latter case behaves similarly to the model B (see Fig. 4).

B. The calculation of C_ℓ

For any fixed pair of values for κ and λ , we take a grid of values of A_i and ϕ_f which span the corresponding upper or lower green/lightly shaded band. For each point on this grid, we consider ϕ_f and its perturbed value, which is found by adding to ϕ_f the amplitude of $\delta\phi_f$ from Eq. (37). We then follow the subsequent evolution

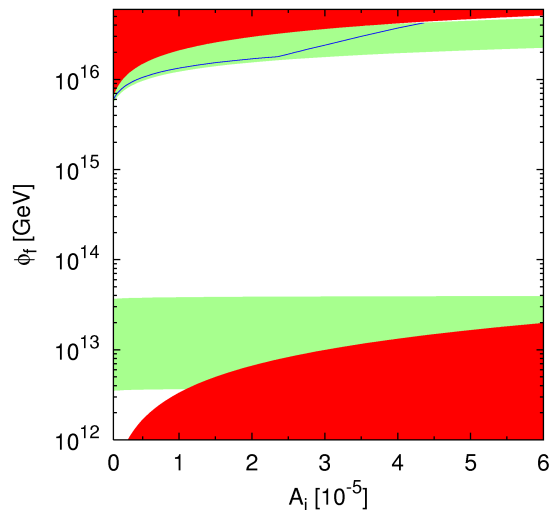


FIG. 4: The two green/lightly shaded bands in the $A_i - \phi_f$ plane which lead to the PQ vacua at t_ϕ for $\kappa = 3 \times 10^{-2}$, $\lambda = 10^{-4}$ (model B). The notation is the same as in Fig. 3.

	Eq.	Model A	Model B
κ	(1)	3×10^{-3}	3×10^{-2}
λ	(2)	10^{-4}	
$m_{3/2}$	(4)	300 GeV	
$ A $	(4)	5	
μ	(6)	300 GeV	
γ	(8)	0 (0.1) during (after) inflation	
T_{reh}	(9)	10^9 GeV	
m_{LSP}	(45)	200 GeV	

TABLE I: Summary of the fixed model parameters for the two representative cases presented in the text, called model A and B. The equation where each parameter first appears is also indicated.

of both these fields until the time t_ϕ of the curvaton decay, where we evaluate the amplitude of $\delta\rho_\phi/\rho_\phi$. The amplitude A_c of the partial curvature perturbation from the curvaton is then given by Eq. (38).

We thus obtain a mapping of the values of ϕ_f which are allowed for any given value of A_i onto the corresponding values of the amplitude A_c of the partial curvature perturbation from the curvaton, which is the relevant variable for the calculation of the CMBR power spectrum. For the MC analysis (see Sec. VIID), we therefore use A_i and A_c as base parameters describing the initial conditions and limit our grid to values of A_i smaller than 6×10^{-5} (since larger values would overpredict the temperature power of the SW plateau). The spectral indices n_i and n_c for each point of this grid are found by using Eqs. (27) and (28) applied at $x = x_Q$, and Eqs. (30), (36) and (39) applied at t_* . The fraction f in Eq. (22) is also evaluated at t_ϕ .

The amplitude A_a of the isocurvature perturbation in the axions is calculated from Eq. (44) with the initial misalignment angle θ evaluated, for any given value of the total CDM abundance $\Omega_{\text{CDM}}h^2 = \Omega_{\text{LSP}}h^2 + \Omega_a h^2$, by using Eqs. (45) and (46) with $m_{\text{LSP}} = 200$ GeV. This value of m_{LSP} corresponds [59], in the constrained MSSM with Yukawa unification [60], roughly to the value of $m_{3/2}$ ($= 300$ GeV) chosen here. Note that, for our choice of parameters, the LSP relic abundance is fixed ($\simeq 0.0074$). The spectral index for axions in each point of the grid is found by using Eq. (47).

In summary, for any fixed pair of values for κ and λ , we take a grid in the variables A_i and ϕ_f covering the upper or lower green/lightly shaded band and numerically map ϕ_f into the corresponding value of the amplitude A_c (which, of course, depends on A_i too). For any value of $\Omega_B h^2$ and $\Omega_a h^2$, we then calculate the amplitudes squared of the adiabatic and isocurvature perturbations using Eqs. (50), (51) and Eqs. (53), (54) respectively, the cross correlation amplitude from Eqs. (55), (56) and the total CMBR temperature and polarization power spectra via Eqs. (58)–(61). The curvaton fractional contribution to the adiabatic amplitude F_c^{ad} , the dimensionless cross correlation $\cos\Delta$ and the entropy-to-adiabatic ratio B are found from Eqs. (52) and (57). For the MC analysis (see Sec. VII D), we need to be able to sample the $A_i - A_c$ space in any point as the chains evolve. Therefore, we perform a 2-dimensional (2D) interpolation between the points on the grid using a bicubic spline. A little care is needed regarding the present value of the Hubble parameter, which enters the computation of the mass scale M and thus H_{infl} for given amplitude A_i via its impact on N_Q (note that the first term in the right hand side of Eq. (32) depends on H_0). As a consequence, the values of the amplitudes A_c and A_a will also depend on the value of H_0 . However, we have found numerically that changing the value of H_0 around $H_0 = 72$ km sec $^{-1}$ Mpc $^{-1}$ within the HST 1σ margin (i.e. by ± 8 km sec $^{-1}$ Mpc $^{-1}$) has an impact less than about 3% on the computed quantities. Therefore, in the computation of M and of the amplitudes A_c and A_a , we fix the present Hubble parameter to the HST central value $H_0 = 72$ km sec $^{-1}$ Mpc $^{-1}$ [56]. Clearly, we do allow H_0 to vary in the MC analysis (see below). In particular, the dependence on H_0 of the amplitudes $A_{P,i}$, $A_{P,c}$ and $A_{P,a}$ at the pivot scale k_P (see Eq. (49)) is taken into account.

C. A toy model for the CMBR

Before deploying the full MC machinery to derive quantitative constraints on the various parameters of our model, it is instructive to consider a toy model for the pre-WMAP CMBR data which allows us to understand the salient qualitative features of the parameter space of our initial conditions. This approach has the great advantage of offering a much more transparent understanding of the parameter constraints beyond the black box of the

numerical MC study.

A first rough idea about the viability of our model can be obtained by using the approximate expressions in Eqs. (62) and (63) for the temperature SW plateau and requiring that the COBE constraint in Eq. (64) is fulfilled. To this end, we take $\Omega_B h^2 = 0.0224$ and $\Omega_{\text{CDM}}h^2 = 0.1126$, which are the best-fit values from the WMAP measurements [2]. (Note that, for this choice of parameters, the axions constitute about 93% of the CDM in the universe.) We find that the COBE constraint cannot be satisfied in the lower green/lightly shaded band in the $A_i - \phi_f$ plane for any pair of values for κ and λ . The reason is that the relatively low values of ϕ_f in this band imply small values for ϕ_* too. The amplitude A_a then turns out to be quite large as can easily be seen from Eq. (44). This fact combined with the sizable relic abundance of the axions leads to large values of S_a (see Eq. (54)), which yield an unacceptably large contribution to the right hand side of Eq. (62). In the upper green/lightly shaded band in the $A_i - \phi_f$ plane, on the contrary, the COBE constraint is generally easily satisfied. The resulting solution is depicted by a blue/solid line (see Figs. 3 and 4).

We are further interested in deriving ball-park estimates for the values of A_i , A_c . To this goal, we again approximate the SW temperature plateau by the expression in Eq. (62). As mentioned, this formula neglects the effect of the cosmological constant Λ (late ISW term), but our present purpose is to build an extremely simplified toy model, not to include all contributions which are fully taken into account in the MC analysis below. Therefore, we take one single datum, namely the COBE constraint in Eq. (64), which describes the height of the SW plateau, along with its variance $\ell(\ell+1)\Delta C_\ell^{\text{TT}}/2\pi|_{\ell=10} \approx 0.2 \times 10^{-10}$ [58]. Furthermore, we drop altogether the dependence of Eq. (62) on the spectral indices by taking all perturbations to be scale invariant, since the value of the indices predicted by our model is anyway very close to unity (see Sec. VII D 2). We need a second datum to be able to constrain two free parameters (A_i and A_c) and this is given by the height of the first adiabatic peak as measured by BOOMERANG [61]. In the analysis of Ref. [62], this yields $\ell(\ell+1)C_\ell^{\text{TT}}/2\pi|_{\ell=212} \approx 5.4 \times 10^{-10}$ with error $\ell(\ell+1)\Delta C_\ell^{\text{TT}}/2\pi|_{\ell=212} \approx 0.54 \times 10^{-10}$. We model the theoretical CMBR spectrum at the level of the first adiabatic peak by retaining the adiabatic contribution only, since the isocurvature temperature spectrum drops very fast beyond the SW plateau. Thus the prediction of our toy PQ model for the height of the first peak is given by

$$C_{212}^{\text{TT,PQ}} \approx \frac{\Delta H}{25} (R_i^2 + R_c^2), \quad (66)$$

where the constant factor $\Delta H \approx 6.5$ approximates the ratio of the first peak height to the SW plateau for the adiabatic temperature spectrum of the standard Λ CDM model. Once again, this expression is very crude and does not account for changes in h , Ω_Λ ($\equiv \rho_\Lambda/\rho_c$ with ρ_Λ being

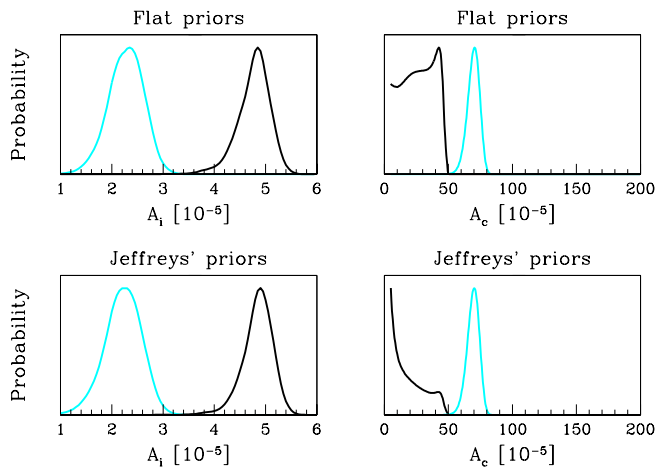


FIG. 5: Posterior marginalized pdf (normalized at peak value) for the amplitudes A_i , A_c from our toy model for two choices of priors: flat priors (top panels), and Jeffreys' priors (bottom panels). The black line is for model A (upper green/lightly shaded band in Fig. 3) and the cyan/light gray line for model B (upper green/lightly shaded band in Fig. 4). The constraints on A_i , A_c in model B and on A_i in model A as well as the upper limit on A_c in model A are robust with respect to the choice of priors. Compare the top panels with Fig. 6, which shows the results of the full MC analysis (with flat non-informative priors).

the dark energy density), Ω_m , Ω_B or τ_r (optical depth to the reionization epoch), all of which affect the relative height of the peak to the plateau, but it is sufficient for our present goal. In summary, the likelihood function $L(A_i, A_c)$ of our toy model is given by

$$-2 \ln L(A_i, A_c) \approx \left(\frac{C_{10}^{\text{TT,PQ}}(A_i, A_c) - C_{10}^{\text{TT}}}{\Delta C_{10}^{\text{TT}}} \right)^2 + \left(\frac{C_{212}^{\text{TT,PQ}}(A_i, A_c) - C_{212}^{\text{TT}}}{\Delta C_{212}^{\text{TT}}} \right)^2, \quad (67)$$

where $C_{10}^{\text{TT,PQ}}$ can be found from Eq. (62). The posterior (see Appendix for definitions) is then

$$\mathcal{P}(A_i, A_c) \propto L(A_i, A_c) \pi(A_i) \pi(A_c). \quad (68)$$

We adopt non-informative flat priors on the amplitudes A_i, A_c , so that $\pi(A_i) = \pi(A_c) = \text{constant}$. An alternative choice is Jeffreys' prior, which is of the form $\pi(A_i) = 1/A_i$, $\pi(A_c) = 1/A_c$ corresponding to a flat prior on $\log A_i, \log A_c$. This prior implies that we do not have any idea on the scale of A_i, A_c before seeing the data and thus represents a quite extreme choice of prior.

In Fig. 5, we present the posterior marginalized probability distribution functions (pdf's) for A_i, A_c from our toy model for the two choices of priors above. We observe that there is a qualitative difference between the results for the upper green/lightly shaded band in Fig. 3 and 4 of model A and B. For model B, both the inflaton

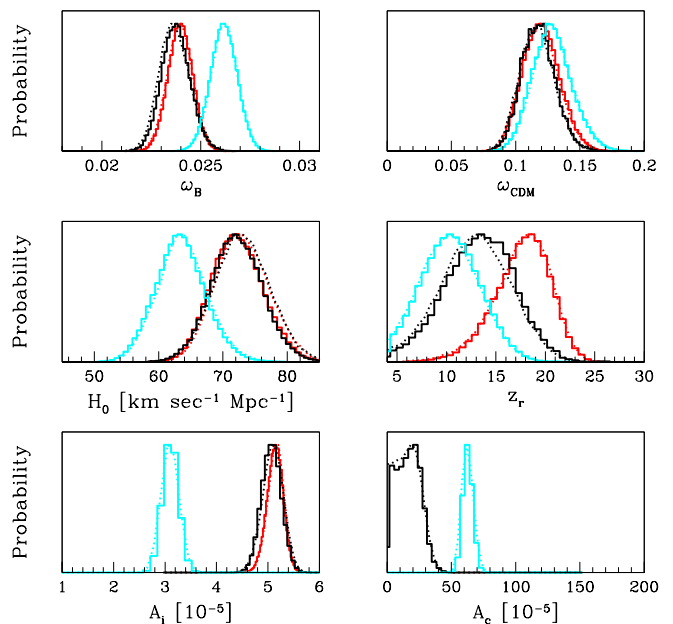


FIG. 6: 1-dimensional (1D) marginalized posterior distribution for the two cases considered here: model A (black solid line) and model B (cyan/light gray solid line) with only the upper green/lightly shaded bands of Figs. 3 and 4 included. The red/medium gray line is for the standard pure inflaton single-field inflationary case with Harrison-Zel'dovich (HZ) spectrum ($n_i = 1.00$ fixed), plotted here for comparison. We plot non-smoothed histograms corresponding to top-hat binnings to show the resolution of our curves. Model A is quite close to the pure inflaton case, except that the curvaton contribution helps in reducing the reionization redshift z_r . Model B displays a preference for non-zero curvaton contribution, a still lower z_r and larger relic abundance of baryons ($\omega_B = \Omega_B h^2$) and CDM ($\omega_{\text{CDM}} = \Omega_{\text{CDM}} h^2$). Its quality of fit is however poorer (see Sec. VIID3 for details). We also display as dotted smoothed curves the values of the mean posterior. All the curves are normalized at their peak value.

and the curvaton amplitude are well determined even in our over-simplified toy model. From the plot, we read off that $A_i \approx 2.3 \times 10^{-5}$, $A_c \approx 70 \times 10^{-5}$. As a consequence, the choice of prior hardly matters, as we would expect in a situation where the posterior is dominated by the likelihood. As for model A, we obtain that $A_i \approx 4.9 \times 10^{-5}$, but we can only place upper limits on the value of A_c . Since, in this case, A_c is not a well-determined parameter, the details of its posterior pdf do depend on the prior. Nevertheless, it is apparent that the upper limit is robust, and we can deduce that $A_i \lesssim 50 \times 10^{-5}$. These numbers have to be taken only as ball-park estimates, and this is why we do not bother to attach errors to them. However, the comparison of Fig. 5 with Fig. 6, which shows the results of the quantitative MC analysis including WMAP and other recent CMBR data and all the other cosmological parameters, displays an astonishing agreement between the results of the above toy model and of the full MC analysis. The rather precise match

of the two results is actually the fortuitous outcome of the cancellation between two opposite effects. On the one hand, the MC analysis compared to the toy model employs much more precise data, which reduce the error on the constraints, but, on the other hand, it also integrates over the cosmological parameter space (totally ignored in the toy model), which enlarges the error on the marginalized quantities.

From the study of the above toy model, we can thus draw two conclusions. First, the height of the first adiabatic peak to the large scale SW plateau is the key quantity to constraining – with at least order of magnitude accuracy – the curvaton to inflaton contribution in the PQ model. Clearly, quantitatively reliable bounds need the inclusion of the detailed effect of the cosmological parameters on the shape of the power spectra (see next section). Second, we have seen that the constraints on the inflaton and curvaton amplitudes are robust with respect to two different choices of (non-informative) priors. For this reason, we will, from now on, adopt a flat prior on A_i , A_c , which will be used both for the extraction of the constraints on the parameters (see Sec. VIID 2) and for the purpose of Bayesian model comparison (see Sec. VIID 3).

D. The Monte Carlo CMBR analysis

1. The setup

We now proceed to describe the setup of the full numerical analysis confronting the predictions of our PQ model with the CMBR data. We constrain the relevant parameters of our model by constructing Markov chains using a modified version of the publicly available Markov chain MC package COSMOMC [63] as described in Ref. [64]. As discussed in Sec. VI, the total CMBR angular power spectrum is given by a (anti-)correlated superposition of adiabatic and isocurvature CMBR modes (see Eq. (58)). The adiabatic and isocurvature CMBR transfer functions are computed in two successive calls similarly to the technique employed in Ref. [65]. For fixed values of κ and λ , the initial conditions are completely specified by A_i and ϕ_f , or equivalently by the values of A_i and A_c as explained in Sec. VII B. The MC sampling takes as free parameters the amplitudes A_i and A_c , the physical baryon and axion densities in the present universe $\omega_B \equiv \Omega_B h^2$ and $\omega_a \equiv \Omega_a h^2$ in units of $1.88 \times 10^{-29} \text{ g/cm}^3$, the present value of the dimensionless Hubble parameter $h = H_0/100 \text{ km sec}^{-1} \text{ Mpc}^{-1}$, and the redshift z_r at which the reionization fraction is a half (assuming sudden reionization). All other derived quantities are computed from the above parameter set, as detailed in Sec. VII B. In particular, the derived parameters R_i^2 , R_c^2 , F_c^{ad} , S_i^2 , S_c^2 , S_a^2 , C_i , C_c are obtained from Eqs. (51), (52), (54) and (56).

For our choice of m_{LSP} and T_{reh} , we have $\Omega_{\text{LSP}} h^2 \approx 0.0074 = \text{constant}$, and the total CDM abundance is

$\omega_{\text{CDM}} \equiv \Omega_{\text{CDM}} h^2 = \Omega_{\text{LSP}} h^2 + \Omega_a h^2$. Our analysis considers flat cosmologies only, thus the cosmological constant energy density Ω_Λ (in units of the critical energy density) is a derived parameter, i.e. $\Omega_\Lambda = 1 - (\omega_{\text{CDM}} + \omega_B)/h^2$. We assume three massless neutrino families and no massive neutrinos (for constraints on these quantities, see e.g. Ref. [66]). We neglect the contribution of gravitational waves to the spectrum, since the tensor to scalar amplitude ratio at the SW plateau is proportional to ϵ_i , which is completely negligible in our case. In summary, for a fixed choice of κ and λ , our parameter space is six dimensional:

$$\theta = \{\omega_B, \omega_a, h, z_r, A_i, A_c\}. \quad (69)$$

We compare the predicted CMBR temperature and polarization power spectra to the WMAP first-year data [2] (temperature and polarization) with the routine for computing the likelihood supplied by the WMAP team [67]. At a smaller angular scale, we add the CBI [32] and the decorrelated ACBAR [30, 31] band powers as well. We then run $N = 20$ Markov chains starting from randomly chosen points in the parameter space. We take particular care in ensuring that the starting points are spread over a wide range in the $A_i - A_c$ plane. We then check that all chains have converged to the same region of parameter space. This indicates that this region is indeed a global minimum (at least for the range explored by the chains). This is the main reason for using a relatively large number of chains, since the danger that the chains are stuck in a local minimum is great when exploring mixed isocurvature initial conditions (see e.g. Ref. [21]). A preliminary run is needed to estimate the covariance matrix, which is then diagonalized and used to perform a final run until each chain contains $M = 30,000$ samples. The mixing of the chains is checked using the Gelman and Rubin criterion [68], for which we require that the ratio of the variance of the mean to the mean of the variance among the chains is $R < 0.1$ for all parameters. The parameter inference is performed on the merged chains, which contain around 5×10^5 samples after the burn-in has been discarded.

As motivated above, we use flat top-hat priors on the base parameters

$$\omega_B, \omega_a, z_r, A_i, A_c. \quad (70)$$

The limits of the top-hat prior do not matter for parameter estimation purposes, as long as we check that the posterior density is negligible near these limits. However, the prior range of the accessible parameter space plays an important role in computing the Bayes factor for model testing (see Sec. VIID 3). We limit the maximum range of the present dimensionless Hubble parameter h by imposing a top-hat prior $0.40 < h < 1.00$ and we use the result of the HST measurement [56]

$$L^{\text{HST}} \propto \exp\left(-\frac{(h - h_0)^2}{2\sigma}\right), \quad (71)$$

param	model A (upper band)		model B (upper band)	
	best fit	1D 68% c.i.	best fit	1D 68% c.i.
ω_B	0.024	0.024 ± 0.002	0.026	0.026 ± 0.002
ω_a	0.109	0.110 ± 0.034	0.117	0.121 ± 0.040
H_0	72.4	$72.2^{+11.5}_{-9.8}$	64.2	$63.4^{+11.0}_{-9.2}$
z_r	13.3	$13.3^{+8.1}_{-9.3}$	10.4	$10.5^{+7.7}_{-6.5}$
$A_i [10^{-5}]$	5.1	5.1 ± 0.5	3.1	3.1 ± 0.4
$A_c [10^{-5}]$	20.3	$< 37.9 (43.2)$	62.0	62.8 ± 10.4
$-\ln L_*$	721.2		732.6	

TABLE II: Best-fit parameter values and sample means with 1σ confidence intervals (c.i.) for the 1D marginalized distribution for the upper band of models A and B. We indicate upper limits only when the parameter is not constrained from below, in which case the first number corresponds to the 68% c.i. (1 tail) and the number in parenthesis to the 95% c.i. of the parameter. The present Hubble parameter H_0 is given in $\text{km sec}^{-1} \text{Mpc}^{-1}$. Finally, L_* is the best-fit likelihood (see Appendix). For comparison, the Harrison-Zel’dovich (HZ) pure inflaton model has $-\ln L_* = 721.7$.

where $h_0 = 0.72$ and $\sigma = 0.08$, by multiplying the likelihood function for the CMBR data by the above Gaussian likelihood.

Parameter constraints will be rather insensitive to the details of the prior distribution whenever the posterior is dominated by the likelihood. As we have seen from our toy model, the broad lines of the constraints for the PQ model are indeed robust with respect to the choice of non-informative priors. We will see below that the priors do play an important role in Bayesian model comparison.

2. Parameter constraints

In the Appendix, we summarize some concepts and results from Bayesian statistics which will be useful in the following analysis (see e.g. Refs. [69] and [70] for reviews and details). We first consider the upper green/lightly shaded band of models A and B. In Tables II and III, we present the best-fit values and parameter constraints obtained from the MC chains for our base and derived parameters respectively. The 1-dimensional (1D) marginalized posterior distributions for the base and most of the derived parameters are plotted, respectively, in Figs. 6 and 7, while the 2D contours of the posterior for A_i , A_c and the adiabatic amplitudes squared R_i^2 , R_c^2 are displayed in Fig. 8.

In the upper (green/lightly shaded) band of model A, the adiabatic amplitude from the inflaton dominates with only a modest contribution ($\sim 10\%$ in amplitude squared) to the adiabatic amplitude from the curvaton and an even smaller curvaton isocurvature amplitude and cross correlator. Note that the axion isocurvature amplitude is negligible in this case. Due to the small value

param	model A (upper band)		model B (upper band)	
	best fit	1D 68% c.i.	best fit	1D 68% c.i.
$R_i^2 [10^{-10}]$	20.4	$21.0^{+6.2}_{-4.2}$	7.8	7.7 ± 2.2
$R_c^2 [10^{-10}]$	2.5	$< 10.9 (14.0)$	14.8	$15.3^{+6.3}_{-4.9}$
$S_i^2 [10^{-10}]$	0.06	0.05 ± 0.04	0.015	0.015 ± 0.006
$S_c^2 [10^{-10}]$	1.2	$< 5.0 (7.1)$	6.6	$6.6^{+3.2}_{-2.1}$
$S_a^2 [10^{-10}]$	0.4	0.4 ± 0.1	6.4	6.3 ± 1.6
$C_i [10^{-10}]$	-1.1	$-1.0^{+0.6}_{-0.5}$	-0.3	-0.3 ± 0.1
$C_c [10^{-10}]$	1.8	$< 6.9 (9.5)$	9.9	$10.0^{+3.6}_{-2.3}$
$\cos \Delta$	0.08	$0.0^{+0.5}_{-0.2}$	0.55	0.56 ± 0.10
B	0.08	$< 0.45 (0.52)$	0.76	0.75 ± 14
F_c^{ad}	0.34	$< 0.60 (0.67)$	0.81	0.81 ± 0.07
f	0.08	$0.07^{+0.02}_{-0.05}$	0.06	0.062 ± 0.004
n_i	0.988	–	0.982	–
n_c	1.011	–	1.003	–
n_a	1.002	–	1.000	–

TABLE III: As in Table II, but for the derived parameters. We do not give c.i. for the spectral indices since the variation in their value is less than 10^{-3} .

of the parameter f , the inflaton part of the isocurvature amplitude squared (correlator) is suppressed relative to the corresponding part of the adiabatic amplitude squared by more than two orders (one order) of magnitude. As a consequence, the power spectra are dominated by the adiabatic part of the inflaton contribution. Moreover, on large scales, we find that the sum of the total power spectrum coming from the curvaton almost cancels out, since the contribution from the curvaton correlator is negative. We can easily verify the behavior just described with the help of Fig. 9, where we plot the best-fit power spectra for model A (upper band) divided into the inflaton, curvaton and axion contributions to their adiabatic, isocurvature and correlator parts. The quality of the fit, as expressed by the maximum likelihood value $-\ln L_* = 721.2$, is slightly better than for the pure inflaton Harrison-Zel’dovich (HZ) case, which has $-\ln L_* = 721.7$ (see, however, our remarks below regarding model comparison). This is not surprising since the curvaton contribution turns out to play a modest role in this model. In particular, the CMBR data put an upper bound on the allowed value of the curvaton amplitude, which is $A_c < 43.2 \times 10^{-5}$ at 95% confidence level (c.l.). The total temperature power on large scales is slightly larger than the pure adiabatic part – the net effect is to increase the height of the SW plateau compared to the height of the first adiabatic peak. This mimics the impact of a larger optical depth (and thus of a larger z_r), and explains why model A shows a preference for a later reionization than in the pure inflaton case. The TE spec-

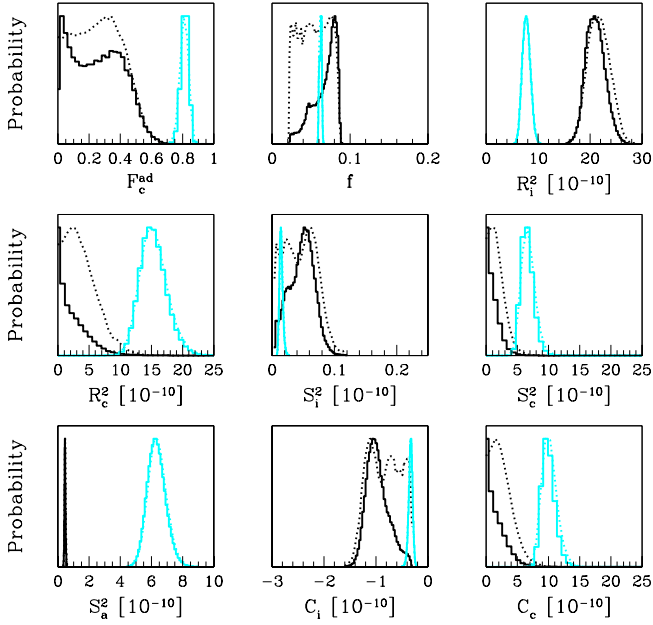


FIG. 7: As in Fig. 6, but for (most of) the derived parameters (the HZ pure inflaton model is not included here). The adiabatic amplitude in model B is dominated by the curvaton ($F_c^{\text{ad}} \approx 0.8$).

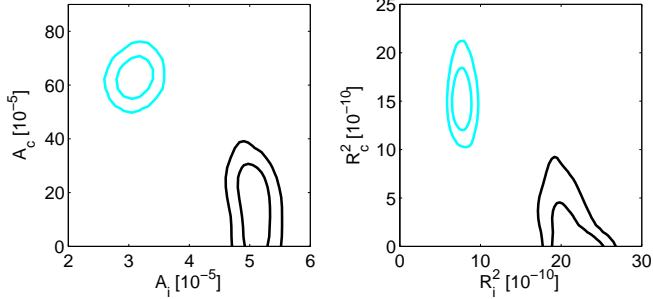


FIG. 8: Contours containing 68% and 95% of the probability for the joint posterior pdf for the upper band of models A and B (same notation as in Fig. 6). The base primordial parameters A_i , A_c are displayed in the left panel, while the right panel shows the derived adiabatic amplitudes squared from the inflaton (R_i^2) and the curvaton (R_c^2). Model B prefers a non-vanishing curvaton contribution to the adiabatic amplitude, but its quality of fit is poorer (see text for details).

trum is dominated by the inflaton adiabatic part, but on large scales the curvaton and axion contributions give a net power increase. This effect helps in better fitting the “reionization bump” (i.e. the power increase for $\ell \lesssim 10$ due to reionization) at low multipoles reducing the need for a rather early reionization.

The upper (green/lightly shaded) band of model B exhibits a preference for a non-vanishing curvaton amplitude with very high significance ($A_c = 62.8 \pm 10.4$) as one can also see from Fig. 8. In this case, the best-fit spectrum is a superposition of a dominant curvaton adi-

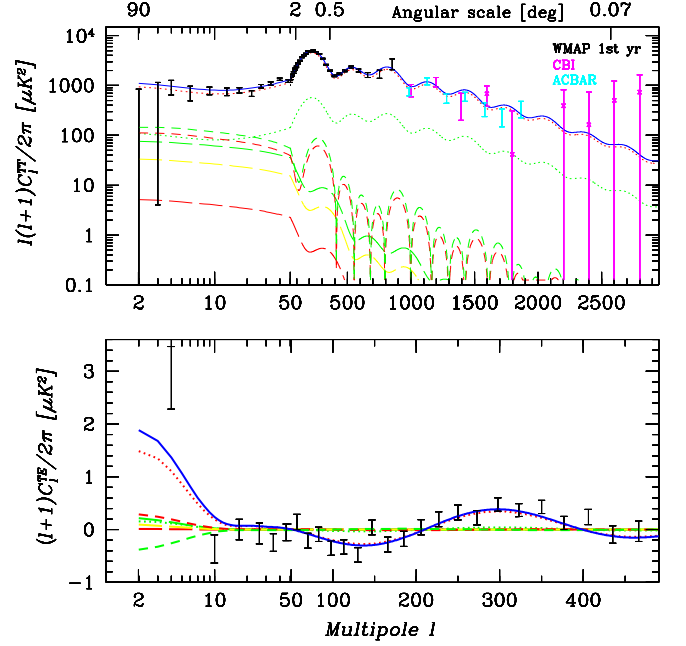


FIG. 9: Best-fit TT (upper panel) and TE (lower panel) power spectra for the upper band of model A (parameters as in Table II). The line codes are: red/dark gray for the inflaton, green/medium gray for the curvaton, and yellow/light gray for the axion contributions; dotted for the adiabatic, long-dashed for the isocurvature, and short-dashed for the correlator parts. The total power corresponds to the blue/solid line. In the upper panel, the correlator parts are given in absolute value. Note though that the inflaton correlator contribution has to be added (negative correlation), while the curvaton one has to be subtracted (positive correlation) to obtain the total power.

adiatic part and an inflaton adiabatic contribution which is around 50% of the former in amplitude squared (see Table III and Fig. 10). This time, the isocurvature curvaton part is sizable on large scales, where however it is again cancelled by the correlator. The large value of κ yields a larger H_* (see Fig. 2) and thus pushes up the axion isocurvature contribution (see Eq. (44)), which again adds power to the SW plateau. As in model A (upper band), the isocurvature and correlator inflaton parts are negligibly small. For the best-fit parameters, the total power in temperature in the COBE region is in better agreement with the data, being slightly smaller than for model A (upper band), thereby fitting better the low-multipole region of the spectrum. However, the overall quality of the fit is worse ($-\ln L_* = 732.6$) because the model does not reproduce with enough precision the shape of the first acoustic peak. We illustrate this in Fig. 11, where we compare the two best-fit spectra for models A and B (upper bands). The WMAP data around the first temperature peak are of such a good quality that they can discriminate between the two models thanks to the slightly different shape of the peak. The reason why the curvaton/inflaton mixture does not

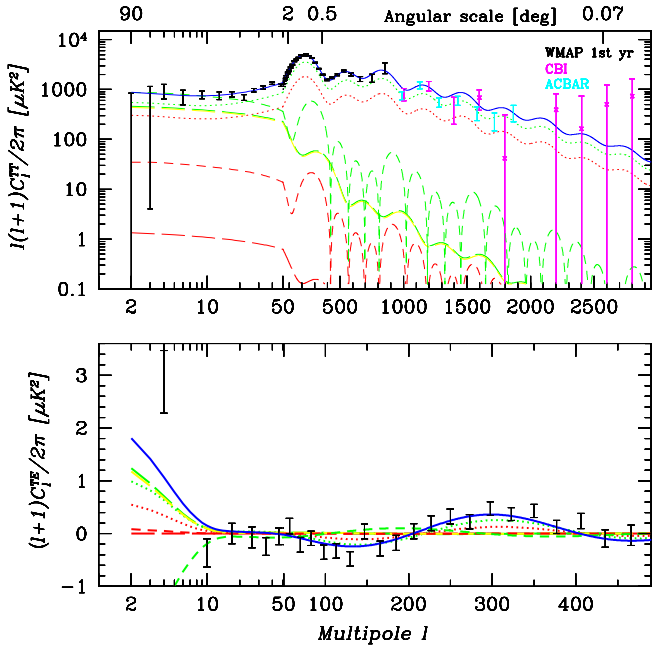


FIG. 10: Best-fit power spectra for the upper band of model B. The base parameters are according to Table II, and the notation is as in Fig. 9.

fit accurately enough the first temperature peak in model B is twofold. First, the isocurvature and correlator contributions are still sizable in the region of the first peak rise ($\ell \sim 100$), and this increases slightly the total power in this part of the spectrum. Second, the curvaton and inflaton have two slightly different spectral indices (see Table III), and the resulting tilts of the spectra are therefore mismatched. As for the TE spectrum, the isocurvature axion part plays an important role in reproducing the reionization bump. Furthermore, model B (upper band) shows a preference for a rather high baryon abundance ($\omega_B \approx 0.026$), which is in strong tension with the value indicated by BBN together with observations of the light elements abundance, which typically yields $\omega_B \approx 0.020 \pm 0.002$ [71].

Fig. 12 shows the 1D marginalized constraints on the dimensionless correlator $\cos \Delta$ and the entropy-to-adiabatic ratio B , while Fig. 13 gives the 2D joint constraints for these two parameters. In model A (upper band), the dominance of the inflaton and the low amplitudes of the correlator modes result in a value of the effective correlation $\cos \Delta$ roughly centered around zero. As discussed above, the entropy contributions play a modest role in model A (upper band), and correspondingly we obtain the upper limit $B \lesssim 0.5$ (at 95% c.l., 1 tail). In model B (upper band), the large amplitude of the curvaton correlator determines a positive total correlation $\cos \Delta \approx 0.5$. Together, the curvaton and axion isocurvature amplitudes constitute a significant fraction of the total amplitude, so that the entropy-to-adiabatic ratio is much larger than zero ($B \approx 0.75$). In summary,

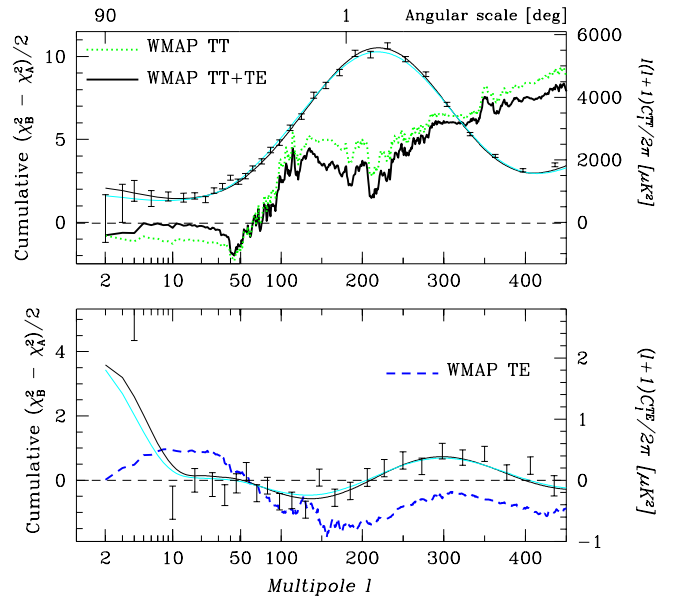


FIG. 11: Cumulative difference between model B and model A (upper bands) of the quantity $\chi^2/2 \equiv -\ln L_*$ for the WMAP TT (green/dotted line in the top panel) and TE data (blue/dashed line in the bottom panel) in units given on the left vertical axes. Their sum is given in the top panel by the thick black solid line. In the top panel, we superimpose the two corresponding best-fit TT spectra for model A (thin black line) and model B (thin cyan/light gray line) with units on the right vertical axis. In the bottom panel, we superimpose the two TE spectra (same notation). To compute the χ^2 difference as a function of the multipole ℓ , we use only the diagonal elements of the data covariance matrix (for the MC analysis, we, of course, included also the off-diagonal elements, which however contribute only a few percent). We also plot the binned WMAP TT (top panel) and TE (bottom panel) errorbars, as a guide to the eye to appreciate the discriminative power of the WMAP data, especially around the first acoustic peak in the temperature spectrum. Model B is a better fit to the TT SW plateau, since its power there is smaller, but its TE spectrum in this region fits the WMAP data worse. Model B cannot reproduce the overall shape of the first acoustic peak in temperature with enough accuracy, and its goodness-of-fit is correspondingly worse.

model B (upper band) shows a complex superposition of modes with a subtly balanced contribution of adiabatic and isocurvature components.

We have also performed a MC analysis for the lower green/lightly shaded band in Fig. 3 of model A. As expected from the arguments given above, the quality of the best fit is poor ($-\ln L_* = 793.4$) as one can see from Table IV and Fig. 14, because the small value of ϕ_* for this band gives rise to a large axion contribution according to Eqs. (44), (49) and (54). Furthermore, the curvaton amplitude A_c turns out to be much larger than the amplitude A_i from the inflaton. This can be understood by observing that, in contrast to A_i , the amplitude A_c from the curvaton can be large and still give a small positive or even a negative contribution to the total power in the

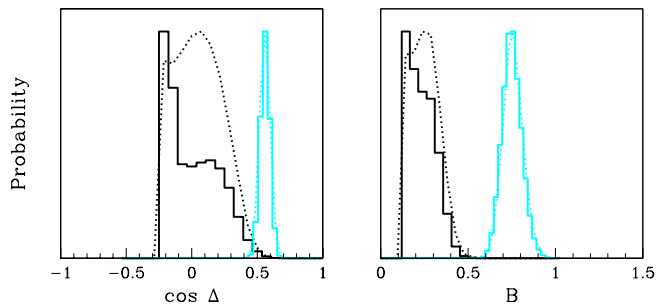


FIG. 12: As in Fig. 6, but for the dimensionless correlator $\cos \Delta$ and the entropy-to-adiabatic ratio B evaluated at the pivot scale k_P (see Eq. (57)). (The HZ pure inflaton model is not included.) The sharp drop for $B \lesssim 0.11$ encountered in model A is a numerical feature due to the lower boundaries of our MC run. The curve must accordingly be interpreted as indicating an upper limit only, which is given in Table III.

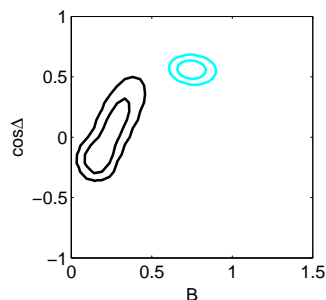


FIG. 13: Contours containing 68% and 95% of the probability for the joint posterior pdf for the upper band of models A and B for the entropy-to-adiabatic ratio B and the dimensionless correlator $\cos \Delta$ (same notation as in Fig. 8).

SW plateau because the curvaton correlation is positive and thus subtracts power from large scales. This is important since, in this case, the axion contribution to the plateau is very large leaving little room for other contributions, while, at smaller scales, the axion isocurvature spectrum becomes negligible and the total temperature spectrum must necessarily be dominated by either the curvaton or the inflaton adiabatic contribution. So one of the two amplitudes A_i or A_c has to be large enough and, as we saw, this can happen only for A_c . Therefore, at smaller scales, the spectrum is dominated by the curvaton adiabatic part. The best-fit inflaton amplitude A_i , on the other hand, corresponds to the lower limit of our parameter space as one can see from Table IV. The reason is that the inflaton contribution to the power spectra is always positive with an unsuppressed (by factors of f or $(\Omega_{\text{LSP}} + \Omega_B)/\Omega_m$) adiabatic part. Thus the inflaton amplitude A_i must be very small in order not to overpredict the large-scale power. Furthermore, the TE spectrum has a very pronounced reionization bump, which results from a rather early reionization epoch and the large axion isocurvature contribution.

The lower band of model B is totally incapable of pro-

param	model A (lower band)	model B (lower band)
ω_B	0.029	0.080
ω_a	0.171	0.010*
H_0	50.1	100.0*
z_r	19.4	30.0*
$A_i [10^{-5}]$	0.10*	0.41
$A_c [10^{-5}]$	75.0	300.0*
$R_i^2 [10^{-10}]$	0.001	0.14
$R_c^2 [10^{-10}]$	33.25	134.1
$S_i^2 [10^{-10}]$	$\sim 10^{-4}$	0.002
$S_c^2 [10^{-10}]$	9.05	971.4
$S_a^2 [10^{-10}]$	14.37	5512.1
$C_i [10^{-10}]$	0.003	0.02
$C_c [10^{-10}]$	17.35	360.9
$\cos \Delta$	0.62	0.39
B	0.84	6.95
F_c^{ad}	1.00	1.00
f	0.077	0.39
n_i	0.986	0.982
n_c	1.000	1.000
n_a	1.000	1.000
$-\ln L_*$	793.4	3014.6

TABLE IV: Best-fit parameter values for the lower band of models A and B. An asterisk indicates that the corresponding parameter has reached the limit of our top-hat prior in the MC run, H_0 is again in $\text{km sec}^{-1} \text{Mpc}^{-1}$ and L_* is the best-fit likelihood. Note that, due to the large value of $\Omega_\Lambda = 0.91$ and the small value of Ω_m in the best fit of model B (lower band), the approximation used in deriving Eq. (62) is no longer valid.

ducing a spectrum in reasonable agreement with the data (see Table IV). For values of A_i , A_c corresponding to this band, the axion contribution is huge and gives temperature fluctuations at large angular scales which are a few orders of magnitude larger than what is observed (see Fig. 15).

Regarding the issue of non-Gaussianity, we note that our parameter f , defined in Eq. (22), is $\gg 10^{-2}$. Therefore, non-Gaussianity from the curvaton partial curvature perturbation is well within the current bounds from WMAP [72] (see Ref. [10]). Actually, the values of f in our model are high enough to ensure that this statement remains true even in the limit of pure curvaton. Moreover, the non-Gaussianity of the isocurvature perturbation in the axions is also negligible. This is because the perturbation $\delta\theta = H_*/2\pi\phi_*$ acquired during inflation by the initial misalignment angle θ (see e.g. Ref. [11]) is always much smaller than θ . As a consequence, terms

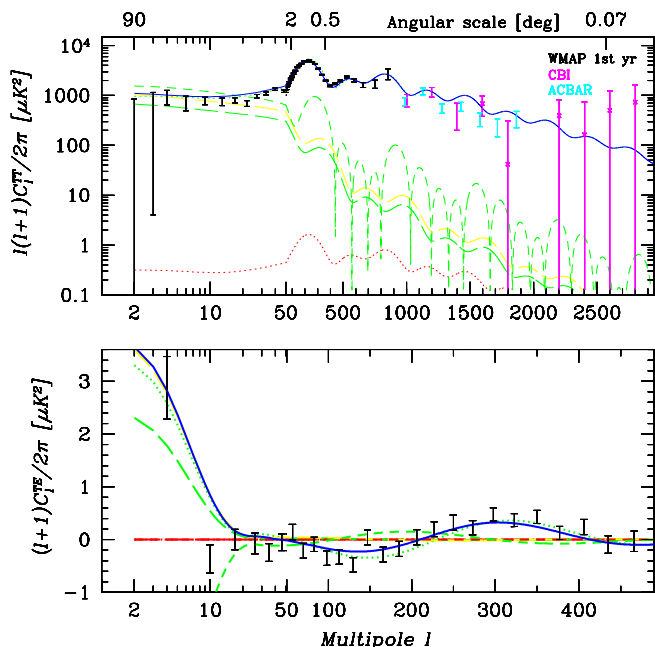


FIG. 14: Best-fit power spectra for the lower band of model A. The base parameters are according to Table IV, and the notation is as in Fig. 9.

which are second order in this perturbation can be safely neglected (see Ref. [73]). Finally, the non-Gaussian component from the inflaton is also negligibly small.

We have performed two other MC runs with the same value for $\lambda = 10^{-4}$ as in model A and κ slightly larger or smaller, i.e. $\kappa = 10^{-2}$ or $\kappa = 10^{-3}$, recovering a behavior which is qualitatively similar to the behavior of model A. We have thus chosen to present our results for this particular value of κ ($= 3 \times 10^{-3}$) as representative of the behavior of this class of models. We have also tried a slightly larger value of λ ($= 3 \times 10^{-4}$) for the same value of $\kappa = 3 \times 10^{-2}$ as in model B, and found a behavior qualitatively similar to model B.

3. Bayesian model comparison

So far we have been concerned with the problem of deriving parameter constraints from the data, given an underlying model for the generation of the primordial fluctuations. Models A and B (upper bands) actually both belong to a continuous class of models (belonging to our PQ model) which is parameterized by κ and λ . However, since in this work we have chosen to fix the values of κ and λ , we may as well consider models A and B (upper bands) as two discrete disconnected models. The question is then to compare these two models with the standard pure inflaton HZ model and decide which of these three models is most favored by data. It should be stressed that model comparison (or model testing) is a different issue than parameter extraction, and indeed it

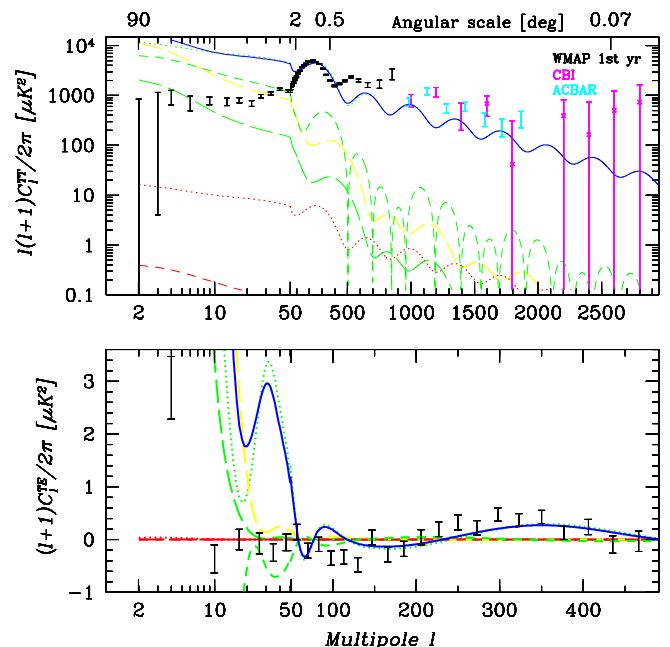


FIG. 15: Best-fit power spectra for the lower band of model B. The base parameters are according to Table IV, and the notation is as in Fig. 9.

represents a further step in Bayesian inference. In fact, it can very well be that model testing arrives at a different conclusion than parameter estimation. Indeed, it can be that the estimated value of a parameter under a model \mathcal{M}_1 is far from the null value predicted by model \mathcal{M}_2 , but \mathcal{M}_1 is disfavored against \mathcal{M}_2 by Bayesian model testing, a fact sometimes called “Bartlett’s paradox” [74]. This is exactly the case for A_c in model B (upper band) compared to the pure inflaton model with flat spectrum of perturbations, as we will show below.

Sampling statistics (i.e. the frequentist approach to parameter estimation) uses the notion of the goodness-of-fit test to assess the viability of a model without the need of specifying an alternative hypothesis. This usually reduces to the χ^2 statistics for the observed data, presuming the model under consideration, \mathcal{M} , is true. \mathcal{M} is then rejected if the value of the goodness-of-fit falls above a certain threshold in the tail of the distribution. If we take this criterion at face value and use the χ^2 statistics for the WMAP data, the best-fit pure inflaton Λ CDM model with $n_s \neq 1$ having $\chi^2 = 1431$ for $\nu = 1342$ degrees of freedom (see last paper in Ref. [2]) would be rejected with a type I error (i.e. probability of falsely rejecting a true model) of about 5%. Notice that this does not mean, as sometimes stated, that “the probability of the model is 5%”. We will see below that Bayesian model comparison is more informative and can give useful guidance for model building.

It is clear that models with a very poor best fit can be discarded simply by inspection. An extreme example is certainly the lower band of model B presented above.

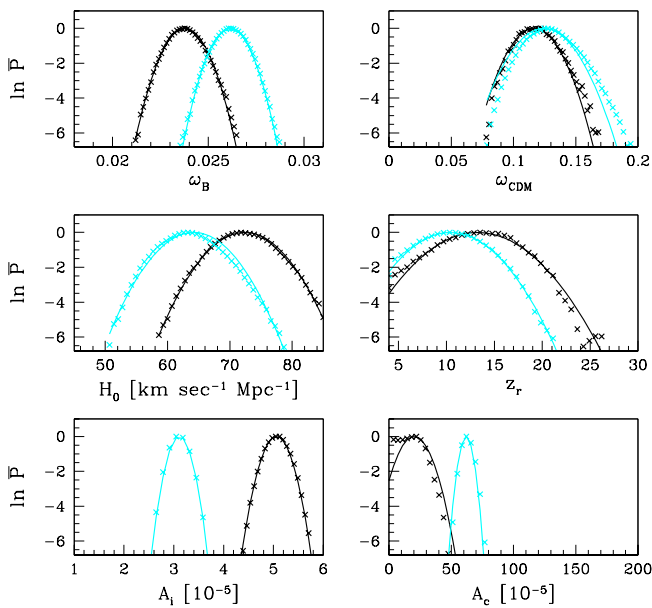


FIG. 16: Illustration of the Laplace approximation to the (non-normalized) posterior used to compute the model evidence. For our base parameters, we plot the logarithm of the 1D marginalized posterior from the MC samples (crosses corresponding to the histograms in Fig. 6) along with the corresponding Laplace approximation (solid smooth lines) of Eq. (A9) for the upper bands of model A (black) and model B (cyan/light gray). Clearly, the Laplace approximation is very good for model B, and of acceptable quality for model A. All the curves are normalized to zero at their peak value. In particular, A_c is a rather non-Gaussian direction for model A (upper band), since the posterior from the MC samples only gives an upper limit on this parameter.

The goodness-of-fit for the lower band of model A is also very poor, even though this is not readily distinguishable from Fig. 14 due to the logarithmic scale. In fact, the best-fit point has $-\ln L_* = 793.4$, compared to $-\ln L_* = 721.2$ for the upper band of this model. Again, we can dismiss the lower band without further analysis. However, we need a more powerful tool if we are to decide, on the basis of the available data, between the viability of our PQ model as opposed to the pure inflaton HZ model. Bayesian inference offers a natural tool for model comparison in the form of the evidence in favor of the model (see Appendix for details and precise definitions).

We thus compute the Bayes factor for models A and B (upper bands), comparing each of them to the scale-invariant (i.e. $n_i = 1.00$) pure inflaton model, which we call in the following the HZ inflation model. We approximate the integrals involved in the evaluation of the Bayes factor by using the Laplace approximation (see Eq. (A9)). We must first check that a multi-dimensional Gaussian is a reasonable approximation to the actual shape of our (non-normalized) posterior pdf. This is shown in Fig. 16, where we plot the logarithm of the 1D marginalized non-

normalized posterior from the MC samples along with the corresponding Laplace approximation. For model B (upper band), the Gaussian approximation is quite accurate along all directions, while for model A (upper band) we notice that A_c is a rather non-Gaussian direction, which is not surprising since this model only gives upper bounds on the amplitude A_c . However, inspection of the figure does seem to support the view that it is reasonably accurate to use the Laplace approximation to compute the model evidence. Another qualitative criterion is the similarity of the marginalized 1D posterior and the mean posterior. If the posterior is a multi-dimensional Gaussian, then the two curves coincide (see e.g. Ref. [64]). From Fig. 6, we can indeed confirm that the two curves are very similar, again strengthening the conclusion that the Laplace approximation is legitimate in our case, more so for model B.

We first compare the upper band of model B (\mathcal{M}_1 in the notation used in the Appendix) against the HZ inflationary case (\mathcal{M}_2), and compute the Bayes factor B_{12} in favor of model B (upper band). The term \mathcal{L}_{12} (see Eq. (A13)) is just the difference of the best-fit log-likelihoods yielding $\mathcal{L}_{12} = -10.9$, and clearly disfavors model B (upper band), whose fit is worse. The term \mathcal{C}_{12} (see Eq. (A14)) describes the ratio of the occupied volumes in parameter space by the posterior pdf's of the two models times a factor taking into account the different dimensionality of the two parameter spaces and is found to be $\mathcal{C}_{12} = 3.0$. Further considerations are needed to evaluate \mathcal{F}_{12} (see Eq. (A15)), the term which reflects the prior available volume of parameter space under each model. In the present case, we do not need to specify the top-hat range of the priors on the parameters which are common to both model B (upper band) and the HZ inflation model. This is because, whatever prior belief we hold about the possible range for these parameters, it will be the same for both models. The parameters common to both models are ω_B , ω_{CDM} , h , z_r and A_i . In the PQ model, the prior range for the CDM abundance actually applies to the axion component of CDM only, but the difference, which is caused by the presence in the universe of the LSPs, is very small and insignificant for our considerations here. Also, we could actually assign to the inflaton amplitude A_i two different prior ranges for the PQ and the HZ inflation models if we had any reason to believe that the ranges can be significantly different in the two cases. Here we take the view that A_i is essentially a free parameter in both models, and thus whatever prior range we assign to it will cancel out from \mathcal{F}_{12} . As a consequence, the only prior range which does not cancel out from \mathcal{F}_{12} is the one for the extra parameter of our PQ model, i.e. A_c . So we have

$$\mathcal{F}_{12} = \ln \frac{1}{\Delta A_c}, \quad (72)$$

where ΔA_c is the top-hat prior range of A_c for the PQ model which is allowed in model B (upper band). The bounds of the prior on A_c correspond to the limits on

	model A (upper band) versus HZ	model B (upper band) versus HZ
\mathcal{L}_{12}	0.5	-10.9
\mathcal{C}_{12}	4.8	3.0
\mathcal{F}_{12}	-9.2	-9.2
$\ln B_{12}$	-3.9	-17.1
posterior odds	1 : 50	1 : 10^7

TABLE V: Results of the Bayes factors analysis for comparing the PQ models A and B (upper bands) to the HZ inflation model. When considering CMBR data only, the odds are in favor of the HZ model against the PQ models. In particular, model B (upper band) is very strongly disfavored.

A_c in the upper band of model B. The lower limit is of no importance, since we can simply set it equal to zero. The upper limit is achieved on the boundary of the upper band, which gives $A_c^{\max} \approx 0.1$. From these considerations and writing A_c in units of 10^{-5} (which are the same units used in the covariance matrix), we have $\Delta A_c \approx 10^4$, and thus $\mathcal{F}_{12} = -9.2$. Putting everything together, we find $\ln B_{12} = -17.1$ and thus the Bayes factor disfavors model B (upper band) against the HZ inflation model with odds of about 10^7 against 1. Notice that the reason for such high odds comes partly from the worse quality of fit of model B (upper band), and partly from an ‘‘Occam’s razor’’ penalty of the PQ model, because it introduces a new scale in the problem (the curvaton amplitude A_c) which has a very wide prior range. We comment further on this aspect below.

We now compute the Bayes factor for the upper band of model A (\mathcal{M}_1) against the HZ inflation model (\mathcal{M}_2). As mentioned above, in this case we expect the Laplace approximation to be less accurate, because A_c is now a non-Gaussian direction. The term \mathcal{L}_{12} is now slightly in favor of model A (upper band), since its fit is marginally better than the one of the HZ inflation model, giving $\mathcal{L}_{12} = 0.5$. From the covariance matrices of the two models, we obtain $\mathcal{C}_{12} = 4.8$, while the same reasoning as above gives again a very small value for \mathcal{F}_{12} as a consequence of the large allowed prior range of A_c , i.e. $\mathcal{F}_{12} = -9.2$. This last term again heavily penalizes the PQ model, resulting in $\ln B_{12} = -3.9$, or odds of 50 : 1 against the PQ model A (upper band). The Laplace approximation is however likely to underestimate the actual volume occupied by the likelihood function in parameter space, due to the fact that A_c is a rather non-Gaussian direction for model A. As a consequence, the above odds can be interpreted as an upper limit for the evidence against model A. We summarize these results on the PQ models A and B (upper bands) in Table V.

One must be very careful when interpreting the above results for the evidence. In fact, the HZ inflationary model, which we used for the comparison, is a natural

benchmark model as far as the CMBR data are concerned. However, one must keep in mind that the PQ model which we describe in this work addresses many fundamental issues which lie outside the scope of the phenomenological HZ inflation model, such as the strong CP and μ problems of MSSM, the generation of the observed BAU and the nature of the CDM in the universe. Our approach was to consider fundamental (SUSY GUT) models of particle physics within the cosmological framework by merging together requirements and constraints both from the particle physics and the cosmology side. In general, it is clear that any viable particle physics model has many free parameters about which little or no experimental information is available at the moment, such as the parameters of the electroweak Higgs sector, the sparticle mass spectrum or the boundary conditions from supergravity which also determine the radiative electroweak symmetry breaking. Nevertheless, we do have some indication about their order of magnitude by applying criteria of simplicity, naturalness and elegance to our fundamental theories. At this stage, the exquisite cosmological data nowadays at our disposal can provide significant constraints on the parameter space of the model. Our evidence calculation, in fact, takes into account only a part of our knowledge (i.e. the CMBR data) neglecting all the other issues which are addressed at a fundamental level by our model. It seems fair to say that, on the whole (i.e. considering both cosmology and particle physics), the PQ model presented in this work aims at a broader explanatory power than a phenomenological inflation model. We thus conclude from our analysis that the present CMBR data can strongly disfavor certain regions of parameter space, as it is the case for model B. In this case, we found robust evidence that a mixture of curvaton and inflaton contributions to the cosmological perturbations is in disagreement with the present CMBR data. On the other hand, the odds against model A should be regarded while keeping in mind the above considerations. In conclusion, it seems to us that, at the present stage, we cannot reject the possibility of a subdominant curvaton contribution to predominantly inflaton-dominated adiabatic perturbations.

On a more phenomenological level, our treatment of the evidence highlights a generic feature of any model which introduces a second (or several) scale-free parameter(s) to describe an extra non-adiabatic component, namely that Occam’s razor of Bayesian model comparison will always penalize such a model with respect to the pure inflaton single-field HZ inflationary model by assigning to it a very small \mathcal{F}_{12} term. This reflects the fact that the extra amplitude parameter (describing an isocurvature contribution) can *a priori* assume any value at all, and therefore there is no hard-wired justification why its value should be smaller than 10^{-5} , or indeed close to but different from zero. So, from a Bayesian point of view, it is certainly unjustified to increase the model’s complexity to achieve only a minuscule gain (if any at all) on the quality of fit. Traditionally, most attention has been

devoted to the maximum likelihood value as the criterion to judge whether a certain new parameter is useful or not. But, from the point of view of model building and Bayesian model testing, restricting the prior volume of parameter space could end up to be as useful, for an inflationary model which would predict the value of A_i to be in the ball-park of 10^{-5} would have very favorable posterior odds against a model in which A_i is essentially a free parameter.

Finally, the example of model B (upper band) above strikingly illustrates that Bayesian “credible intervals” cannot be interpreted as “significance levels”, for, just by looking at the constraints on the amplitude A_c for the upper band of model B, one could have (erroneously) deduced a 6σ detection of a non-zero curvaton amplitude. Clearly, from the poor quality of the best fit ($-\ln L_* = 732.6$), it would have been immediately obvious, without the need of computing the Bayes factor, that this particular model could not be favored by data. However, the conceptual point remains: the question whether a certain parameter value differs from the null reference value cannot be answered by looking at the confidence intervals (c.i.), but must be tackled by proper model comparison procedures. While this point is certainly clear to data analysts working in the field, it seems appropriate to stress it once more in view of a widespread misinterpretation of this concept.

VIII. CONCLUSIONS

We considered a simple and concrete SUSY GUT model which automatically and naturally solves the strong CP and μ problems of MSSM via a PQ and a continuous R symmetry. This model also leads to the standard SUSY realization of hybrid inflation. The PQ field of this model, which corresponds to a flat direction in field space lifted by non-renormalizable interactions, can act as curvaton contributing together with the inflaton to the total curvature perturbation in the universe. In contrast to the standard curvaton hypothesis, we did not suppress the contribution from the inflaton.

The CDM in the universe predicted by this model consists predominantly of axions which are produced at the QCD phase transition. It also contains LSPs originating from the gravitinos which were thermally produced at reheating and decayed well after BBN. For simplicity, we assumed that there are no thermally produced LSPs in the model. The baryons, which are generated via a primordial leptogenesis occurring at reheating, as well as the LSPs inherit the partial curvature perturbation of the inflaton. This is different from the total curvature perturbation, which receives a contribution from the curvaton too. Therefore, the baryons and LSPs carry also an isocurvature perturbation, whose correlation with the total curvature perturbation is mixed. The axions, as usual, contribute only to the isocurvature perturbation. The resulting total isocurvature perturbation has mixed

correlation with the adiabatic one.

Most of the parameters of the model but two were chosen by using criteria of naturalness and simplicity. We considered two representative cases for the two remaining parameters, κ and λ , and compared the predictions with the first-year WMAP observations and other CMBR measurements. We found that, in one of the two cases (model B), the curvaton and axions contributions to the CMBR power spectra are important, and that this leads to a significant disagreement with the data. In fact, Bayesian model comparison disfavors this case as compared to the scale-invariant pure inflaton model with odds of 10^7 against 1. The other possibility which we studied (model A) predicts a predominantly adiabatic power spectrum from the inflaton, where the curvaton and axions contributions are subdominant. We derived upper bounds for the amplitude of the partial curvature perturbation from the curvaton in this case ($A_c \lesssim 43.2 \times 10^{-5}$ at 95% c.l.), and noticed that the interplay of the non-inflaton contributions results in a later reionization redshift ($z_r = 13.3^{+8.1}_{-9.3}$ at 68% c.l.). Even though the best-fit likelihood for this case ($-\ln L_* = 721.2$) is better than in the pure inflaton HZ case, evaluation of the evidence under the Laplace approximation gives odds of about 50 to 1 against model A compared to the pure inflaton HZ case. These odds must be interpreted with caution, since they do not take into account the fact that the PQ model aims at a more fundamental explanatory power and that it addresses many particle physics issues which are outside the scope of inflationary models.

In summary, we have shown that certain regions of the parameter space ($\kappa \approx 3 \times 10^{-2}$ and $10^{-4} \lesssim \lambda \lesssim 3 \times 10^{-4}$) can be excluded on the grounds of present-day CMBR observations. Quantitative bounds on the allowed values of κ and λ could be derived by treating them as free parameters in the MC analysis, an exploration left for future work. Our approach – embedding particle physics model building in the cosmological framework – pursued the issue of merging together fundamental theories and cosmological constraints in a realistic and viable model for the generation of the cosmological perturbations. It is encouraging that modern cosmological observations are now informative enough as to give useful and robust guidance along this path.

ACKNOWLEDGMENTS

We thank K. Dimopoulos, R. Durrer, S. Leach, D. Lyth, Ch. Ringeval, M. Sakellariadou and D. Wands for useful discussions. We are particularly grateful to K. Dimopoulos and D. Lyth for communicating to us their results on the randomization regime for the curvaton field prior to publication. This work was supported by the European Union under RTN contracts HPRN-CT-2000-00148 and HPRN-CT-2000-00152 and was performed on the Myri cluster owned and operated by the University

of Geneva. R.T. was partially supported by the European Network CMBNet and the Swiss National Science Foundation.

APPENDIX A: BAYESIAN INFERENCE: A PRIMER

1. Bayesian parameter estimation

Bayesian inference is based on Bayes' theorem, which is nothing more than rewriting the definition of conditional probability:

$$\mathcal{P}(A|B) = \frac{\mathcal{P}(B|A)\mathcal{P}(A)}{\mathcal{P}(B)} \quad (\text{Bayes' theorem}). \quad (\text{A1})$$

In order to clarify the meaning of this relation, let us write $\boldsymbol{\theta}$ (a vector of d parameters under a model \mathcal{M}) for A and \mathbf{D} (the data at hand) for B , obtaining

$$\begin{aligned} \mathcal{P}(\boldsymbol{\theta}|\mathbf{D}, \mathcal{M}) &= \frac{L(\mathbf{D}|\boldsymbol{\theta}, \mathcal{M})\pi(\boldsymbol{\theta}, \mathcal{M})}{\int_{\Omega} L(\mathbf{D}|\boldsymbol{\theta}, \mathcal{M})\pi(\boldsymbol{\theta}, \mathcal{M})d\boldsymbol{\theta}} \\ &= \frac{L(\mathbf{D}|\boldsymbol{\theta}, \mathcal{M})\pi(\boldsymbol{\theta}, \mathcal{M})}{\mathcal{P}(\mathbf{D}|\mathcal{M})}, \end{aligned} \quad (\text{A2})$$

where Ω designates the parameter space (of dimensionality d) under model \mathcal{M} . This equation relates the *posterior probability* $\mathcal{P}(\boldsymbol{\theta}|\mathbf{D}, \mathcal{M})$ for the parameters $\boldsymbol{\theta}$ of the model \mathcal{M} given the data \mathbf{D} to the *likelihood function* $L(\mathbf{D}|\boldsymbol{\theta}, \mathcal{M})$ if the *prior probability distribution function* $\pi(\boldsymbol{\theta}, \mathcal{M})$ for the parameters under the model is known. The latter is called ‘‘prior’’ for short. The quantity in the denominator is independent of $\boldsymbol{\theta}$ and is called the *evidence* of the data for the model \mathcal{M} [69]. The evidence is the central quantity for model comparison, as we explain below, but, in the context of parameter estimation within a model, it is just an overall multiplicative constant which does not matter. In short,

$$\text{posterior} = \frac{\text{likelihood} \times \text{prior}}{\text{evidence}}. \quad (\text{A3})$$

The prior distribution contains all the knowledge about the parameters before observing the data, i.e. our physical understanding of the model, our insight into the experimental setup and its performance, and in short all our prior scientific experience. This information is then updated via Bayes' theorem to the posterior distribution by multiplying the prior with the likelihood function which contains the information coming from the data. The posterior probability is the base for inference about $\boldsymbol{\theta}$. The most probable value for the parameters is the one for which the posterior probability is largest.

Bayes' postulate states that, in the absence of other arguments, the prior probability should be assumed to be equal for all values of the parameters over a certain range ($\boldsymbol{\theta}_{\min} \leq \boldsymbol{\theta} \leq \boldsymbol{\theta}_{\max}$). This is called a ‘‘flat prior’’,

i.e.

$$\pi(\boldsymbol{\theta}, \mathcal{M}) = [H(\boldsymbol{\theta} - \boldsymbol{\theta}_{\min})H(\boldsymbol{\theta}_{\max} - \boldsymbol{\theta})] \prod_{j=1}^d \frac{1}{\Delta\theta_j}, \quad (\text{A4})$$

where H is the Heaviside step function and $\Delta\theta_j \equiv \theta_{\max,j} - \theta_{\min,j} > 0, \forall j$. Clearly, a flat prior on $\boldsymbol{\theta}$ does not correspond to a flat prior on some other set $\boldsymbol{\alpha}(\boldsymbol{\theta})$ obtained via a non-linear transformation, since the two prior distributions are related via

$$\pi(\boldsymbol{\theta}, \mathcal{M}) = \pi(\boldsymbol{\alpha}, \mathcal{M}) \frac{d\boldsymbol{\alpha}(\boldsymbol{\theta})}{d\boldsymbol{\theta}}. \quad (\text{A5})$$

A recurrent criticism is that the final inference depends on the prior which one chooses to use. However, in a situation in which the data exhibit a clear preference for a certain value for a parameter, the posterior is effectively dominated by the likelihood, and the choice of prior will not matter much. This is currently the case, as far as the CMBR is concerned, for high ‘‘signal to noise’’ parameters such as the baryon density. Constraints on other parameters such as the curvaton amplitude A_c in model A (upper band) of our PQ scenario are likely to depend slightly on the details of the chosen prior distribution. In other words, constraints on parameters which are not clearly determined will suffer from a certain degree of subjectivity, depending on what prior $\pi(\boldsymbol{\theta}, \mathcal{M})$ we choose on the right hand side of Eq. (A2). This fact should be interpreted as a warning, telling us that the data are not powerful enough to clearly single out the parameter under consideration.

2. Bayes factors

Let us consider two competing models \mathcal{M}_1 and \mathcal{M}_2 and ask what is the posterior probability of each model given the data \mathbf{D} . By Bayes' theorem we have

$$\mathcal{P}(\mathcal{M}_i|\mathbf{D}) \propto \mathcal{P}(\mathbf{D}|\mathcal{M}_i)\pi(\mathcal{M}_i) \quad (i = 1, 2), \quad (\text{A6})$$

where $\mathcal{P}(\mathbf{D}|\mathcal{M}_i)$ is the evidence of the data under model \mathcal{M}_i and $\pi(\mathcal{M}_i)$ is the prior probability of the i th model before we see the data. The ratio of the posterior odds for the two competing models is called *Bayes factor* [75]:

$$B_{12} \equiv \frac{\mathcal{P}(\mathcal{M}_1|\mathbf{D})}{\mathcal{P}(\mathcal{M}_2|\mathbf{D})}. \quad (\text{A7})$$

Usually, we do not hold any prior beliefs about the two models and therefore $\pi(\mathcal{M}_1) = \pi(\mathcal{M}_2) = 1/2$, so that the Bayes factor reduces to the ratio of the evidences. The Bayes factor can be interpreted as an automatic Occam's razor, which disfavors complex models involving many parameters (see Ref. [69] for details) as we discuss below and demonstrate in the text.

The evidence in favor of \mathcal{M} can be evaluated by performing the integral

$$\begin{aligned} \mathcal{P}(\mathbf{D}|\mathcal{M}) &= \int_{\Omega} L(\mathbf{D}|\boldsymbol{\theta}, \mathcal{M})\pi(\boldsymbol{\theta}, \mathcal{M})d\boldsymbol{\theta} \\ &= \int_{\Omega} \bar{\mathcal{P}}(\boldsymbol{\theta}|\mathbf{D}, \mathcal{M})d\boldsymbol{\theta}, \end{aligned} \quad (\text{A8})$$

where $\bar{\mathcal{P}}(\boldsymbol{\theta}|\mathbf{D}, \mathcal{M})$ designates the non-normalized posterior probability (i.e. the numerator in the right hand side of Eq. (A2)). Computing the above integral from the MC samples is difficult, since there will be very few or no samples in the tails of the likelihood. There are however a number of approximate methods which can be applied [76]. Most of them rely on the fact that, for a large number of data points, the likelihood function will tend to be a multi-dimensional Gaussian distribution. One simple approximation is then to expand the logarithm of the non-normalized posterior to second order around its peak, which (for flat prior) occurs at the best-fit parameter choice $\boldsymbol{\theta}_*$, where the likelihood is maximized. We obtain

$$\ln \frac{\bar{\mathcal{P}}(\boldsymbol{\theta}|\mathbf{D}, \mathcal{M})}{\bar{\mathcal{P}}(\boldsymbol{\theta}_*|\mathbf{D}, \mathcal{M})} \approx -\frac{1}{2}(\boldsymbol{\theta} - \boldsymbol{\theta}_*)^T \mathbf{C}^{-1}(\boldsymbol{\theta} - \boldsymbol{\theta}_*), \quad (\text{A9})$$

where \mathbf{C} is the covariance matrix of the model \mathcal{M} evaluated at the best-fit point, which can be estimated from the MC samples. This is called Laplace approximation and can be expected to give sensible results if the non-normalized posterior is reasonably well described by the multi-dimensional Gaussian Eq. (A9). It is then straightforward to evaluate the evidence by using the approximate form in Eq. (A9) for the non-normalized posterior, obtaining

$$\begin{aligned} \mathcal{P}(\mathbf{D}|\mathcal{M}) &= \int_{\Omega} \bar{\mathcal{P}}(\boldsymbol{\theta}|\mathbf{D}, \mathcal{M})d\boldsymbol{\theta} \\ &\approx (2\pi)^{\frac{d}{2}} \bar{\mathcal{P}}(\boldsymbol{\theta}_*|\mathbf{D}, \mathcal{M}) \sqrt{\det \mathbf{C}}. \end{aligned} \quad (\text{A10})$$

For flat separable priors of the form in Eq. (A4) we can simply write, abbreviating $\Delta\boldsymbol{\theta} \equiv \prod_{j=1}^d \Delta\theta_j$,

$$\bar{\mathcal{P}}(\boldsymbol{\theta}_*|\mathbf{D}, \mathcal{M}) = L(\mathbf{D}|\boldsymbol{\theta}_*, \mathcal{M}) \frac{1}{\Delta\boldsymbol{\theta}}, \quad (\text{A11})$$

an expression which is still approximately correct even if we used non-flat priors, and interpret $\Delta\theta_j$ as the typical width of the prior pdf (say the standard deviation along the direction of the j th parameter for a Gaussian distributed prior). For a Gaussian prior, it is easy to derive an exact expression analogous to Eq. (A11), but for simplicity we will stick to the above form.

For the logarithm of the Bayes factor in the Laplace approximation, we finally obtain the following handy expression:

$$\ln B_{12} \approx \mathcal{L}_{12} + \mathcal{C}_{12} + \mathcal{F}_{12}, \quad (\text{A12})$$

where we have defined

$$\mathcal{L}_{12} \equiv \ln \frac{L(\mathbf{D}|\boldsymbol{\theta}_*^{(1)}, \mathcal{M}_1)}{L(\mathbf{D}|\boldsymbol{\theta}_*^{(2)}, \mathcal{M}_2)}, \quad (\text{A13})$$

$$\mathcal{C}_{12} \equiv \frac{1}{2} \left(\ln \left[(2\pi)^{d^{(1)} - d^{(2)}} \right] + \ln \frac{\det \mathbf{C}^{(1)}}{\det \mathbf{C}^{(2)}} \right), \quad (\text{A14})$$

$$\mathcal{F}_{12} \equiv \ln \frac{\Delta\boldsymbol{\theta}^{(2)}}{\Delta\boldsymbol{\theta}^{(1)}}, \quad (\text{A15})$$

where quantities referring to the model \mathcal{M}_i ($i = 1, 2$) are indicated by a superscript (i). The term \mathcal{L}_{12} is the logarithm of the ratio of the best-fit likelihoods. From a frequentist point of view, this quantity is approximately χ^2 distributed, and thus it is common practice to apply to it a goodness-of-fit test to assess whether the extra parameters have produced a “significant” increase of the quality of fit. If the model \mathcal{M}_1 contains more parameters than the model \mathcal{M}_2 , then \mathcal{M}_1 should show an improved fit to the data, i.e. we should have $\mathcal{L}_{12} > 0$, unless the extra parameters are useless, in which case $\mathcal{L}_{12} = 0$. In any case, a goodness-of-fit test alone does not say anything about the structure of the parameter space for the model under consideration, since it is limited to the maximum likelihood point. But Bayesian evidence does contain two further pieces of information, \mathcal{C}_{12} and \mathcal{F}_{12} , which taken together are sometimes referred to as “Occam’s factor”. Here we prefer to consider these terms separately to help distinguishing their different origin. The term \mathcal{C}_{12} describes the structure of the posterior shape in the Gaussian approximation. Since the determinant is the product of the eigenvalues of the covariance matrix, which represent the standard deviations squared along the corresponding eigenvectors in the parameter space of the model, it follows that if \mathcal{M}_1 has a narrower posterior than \mathcal{M}_2 , then $\mathcal{C}_{12} < 0$, thereby disfavoring \mathcal{M}_1 . This apparent contradiction (how can a model with smaller errors display a smaller evidence?) is resolved when we take into account the term \mathcal{F}_{12} , which describes the prior available parameter space under each model. The sum of the terms \mathcal{C}_{12} and \mathcal{F}_{12} thus disfavors the model with the largest volume of “wasted” parameter space when the data arrive. A more complex model \mathcal{M}_1 – having a large number of parameters and thus a large volume of prior accessible parameter space – will naturally fit the data better due to its flexibility, i.e. we will have $\mathcal{L}_{12} > 0$, but it will be penalized for introducing extra dimensions in parameter space, i.e. the sum $\mathcal{C}_{12} + \mathcal{F}_{12}$ will be negative. In summary, the Bayes factor tends to select the model which exhibits an optimal trade-off between simplicity and quality of fit.

It should be clear that the choice of priors plays an important role in Bayesian model comparison (testing) via its impact on the term \mathcal{F}_{12} . In particular, prior pdf’s used in evaluating the Bayes factor must be proper, i.e. normalizable, so that we can impose the normalization condition

$$\int_{\Omega} \pi(\boldsymbol{\theta}, \mathcal{M})d\boldsymbol{\theta} = 1. \quad (\text{A16})$$

Although generally a strong dependence on the choice of priors is regarded as suspicious, in this case, we should consider the role of \mathcal{F}_{12} as a way to implement *a priori*

model features into the Bayes factor, as we show in the text of the paper.

-
- [1] A. Guth, Phys. Rev. D **23**, 347 (1981).
- [2] C.L. Bennett *et al.*, Astrophys. J. Suppl. **148**, 1 (2003); G. Hinshaw *et al.*, *ibid.* **148**, 135 (2003); A. Kogut *et al.*, *ibid.* **148**, 161 (2003); D.N. Spergel *et al.*, *ibid.* **148**, 175 (2003).
- [3] H.V. Peiris *et al.*, Astrophys. J. Suppl. **148**, 213 (2003).
- [4] A.R. Liddle and D.H. Lyth, *Cosmological inflation and large-scale structure* (Cambridge University Press, Cambridge, U.K., 2000).
- [5] G. Lazarides, Lect. Notes Phys. **592**, 351 (2002) [hep-ph/0111328]; hep-ph/0204294.
- [6] C. Gordon and A. Lewis, Phys. Rev. D **67**, 123513 (2003); P. Crotty, J. García-Bellido, J. Lesgourgues and A. Riazuelo, Phys. Rev. Lett. **91**, 171301 (2003); M. Bucher, J. Dunkley, P.G. Ferreira, K. Moodley and C. Skordis, *ibid.* **93**, 081301 (2004); K. Moodley, M. Bucher, J. Dunkley, P.G. Ferreira and C. Skordis, astro-ph/0407304.
- [7] N. Bartolo, E. Komatsu, S. Matarrese and A. Riotto, astro-ph/0406398.
- [8] S. Mollerach, Phys. Rev. D **42**, 313 (1990); A.D. Linde and V. Mukhanov, *ibid.* **56**, 535 (1997).
- [9] D.H. Lyth and D. Wands, Phys. Lett. B **524**, 5 (2002); T. Moroi and T. Takahashi, *ibid.* **522**, 215 (2001); **539**, 303(E) (2002).
- [10] D.H. Lyth, C. Ungarelli and D. Wands, Phys. Rev. D **67**, 023503 (2003).
- [11] K. Dimopoulos, G. Lazarides, D. Lyth and R. Ruiz de Austri, J. High Energy Phys. **05**, 057 (2003).
- [12] K. Dimopoulos and D.H. Lyth, Phys. Rev. D **69**, 123509 (2004).
- [13] G. Lazarides and Q. Shafi, Phys. Rev. D **58**, 071702 (1998).
- [14] R. Peccei and H. Quinn, Phys. Rev. Lett. **38**, 1440 (1977); S. Weinberg, *ibid.* **40**, 223 (1978); F. Wilczek, *ibid.* **40**, 279 (1978).
- [15] E.J. Copeland, A.R. Liddle, D.H. Lyth, E.D. Stewart and D. Wands, Phys. Rev. D **49**, 6410 (1994).
- [16] G. Dvali, Q. Shafi and R. Schaefer, Phys. Rev. Lett. **73**, 1886 (1994).
- [17] A.D. Linde, Phys. Lett. B **259**, 38 (1991); Phys. Rev. D **49**, 748 (1994).
- [18] C.L. Bennett *et al.*, Astrophys. J. **464**, L1 (1996).
- [19] J.E. Kim and H.P. Nilles, Phys. Lett. B **138**, 150 (1984).
- [20] C. Gordon and K.A. Malik, Phys. Rev. D **69**, 063508 (2004); M. Beltrán, J. García-Bellido, J. Lesgourgues and A. Riazuelo, astro-ph/0409326.
- [21] E. Pierpaoli, J. García-Bellido and S. Borgani, J. High Energy Phys. **10**, 015 (1999); R. Trotta, A. Riazuelo and R. Durrer, Phys. Rev. Lett. **87**, 231301 (2001); Phys. Rev. D **67**, 063520 (2003).
- [22] L. Amendola, C. Gordon, D. Wands and M. Sasaki, Phys. Rev. Lett. **88**, 211302 (2002).
- [23] D. Langlois and F. Vernizzi, astro-ph/0403258; F. Ferrer, S. Räsänen and J. Väliviita, astro-ph/0407300.
- [24] G. Lazarides and N.D. Vlachos, Phys. Lett. B **459**, 482 (1999).
- [25] G. Lazarides and Q. Shafi, Phys. Lett. B **258**, 305 (1991); G. Lazarides, R.K. Schaefer and Q. Shafi, Phys. Rev. D **56**, 1324 (1997).
- [26] M. Fukugita and T. Yanagida, Phys. Lett. B **174**, 45 (1986).
- [27] M. Dine, W. Fischler and D. Nemeschansky, Phys. Lett. B **136**, 169 (1984); G.D. Coughlan, R. Holman, P. Ramond and G.G. Ross, *ibid.* **140**, 44 (1984).
- [28] M. Dine, L. Randall and S. Thomas, Phys. Rev. Lett. **75**, 398 (1995); Nucl. Phys. **B458**, 291 (1996).
- [29] E.D. Stewart, Phys. Rev. D **51**, 6847 (1995); M.K. Gaillard, H. Murayama and K.A. Olive, Phys. Lett. B **355**, 71 (1995); M.K. Gaillard, D.H. Lyth and H. Murayama, Phys. Rev. D **58**, 123505 (1998); C. Panagiotakopoulos, Phys. Lett. B **459**, 473 (1999); R. Jeannerot, S. Khalil and G. Lazarides, J. High Energy Phys. **07**, 069 (2002).
- [30] J.H. Goldstein *et al.*, Astrophys. J. **599**, 773 (2003); C.-I. Kuo *et al.*, *ibid.* **600**, 32 (2004).
- [31] <http://cosmologist.info/ACBAR>.
- [32] T.J. Pearson *et al.*, Astrophys. J. **591**, 556 (2003).
- [33] G. Lazarides, PRHEP-trieste99/008 [hep-ph/9905450].
- [34] G. Lazarides, C. Panagiotakopoulos and Q. Shafi, Phys. Rev. Lett. **56**, 432 (1986).
- [35] N. Ganoulis, G. Lazarides and Q. Shafi, Nucl. Phys. **B323**, 374 (1989); G. Lazarides and Q. Shafi, *ibid.* **B329**, 182 (1990).
- [36] G. Lazarides and C. Panagiotakopoulos, Phys. Rev. D **52**, 559 (1995).
- [37] R. Jeannerot, S. Khalil, G. Lazarides and Q. Shafi, J. High Energy Phys. **10**, 012 (2000).
- [38] G. Lazarides, M. Magg and Q. Shafi, Phys. Lett. B **97**, 87 (1980).
- [39] T.W.B. Kibble, G. Lazarides and Q. Shafi, Phys. Lett. B **113**, 237 (1982).
- [40] R. Jeannerot, J. Rocher and M. Sakellariadou, Phys. Rev. D **68**, 103514 (2003).
- [41] J. Rocher and M. Sakellariadou, hep-ph/0405133.
- [42] K. Dimopoulos, G. Lazarides, D. Lyth and R. Ruiz de Austri, Phys. Rev. D **68**, 123515 (2003).
- [43] J.R. Ellis, J.E. Kim and D.V. Nanopoulos, Phys. Lett. B **145**, 181 (1984); J.R. Ellis, D.V. Nanopoulos and S. Sarkar, Nucl. Phys. **B259**, 175 (1985); J.R. Ellis, G.B. Gelmini, J.L. Lopez, D.V. Nanopoulos and S. Sarkar, *ibid.* **B373**, 399 (1992).
- [44] R.J. Scherrer and M.S. Turner, Phys. Rev. D **31**, 681 (1985).
- [45] G. Lazarides, in *Recent developments in particle physics and cosmology*, edited by G.C. Branco, Q. Shafi and J.I. Silva-Marcos (Kluwer Academic Publishers, Dordrecht, 2001), p. 399 [hep-ph/0011130]; R. Jeannerot, S. Khalil and G. Lazarides, in *The proceedings of Cairo international conference on high energy physics*, edited by S. Khalil, Q. Shafi and H. Tallat (Rinton Press Inc., Princeton, 2001), p. 254 [hep-ph/0106035].
- [46] K. Dimopoulos and D.H. Lyth, private communication.

- [47] K. Dimopoulos, D.H. Lyth, A. Notari and A. Riotto, *J. High Energy Phys.* **07**, 053 (2003).
- [48] D.H. Lyth and E.D. Stewart, *Phys. Rev. D* **46**, 532 (1992).
- [49] K. Dimopoulos and D.H. Lyth, in preparation.
- [50] R. Allahverdi, B.A. Campbell and J.R. Ellis, *Nucl. Phys.* **B579**, 355 (2000); A. Anisimov and M. Dine, *ibid.* **B619**, 729 (2001).
- [51] R. Trotta, *Cosmic microwave anisotropies: beyond standard parameters* (Ph.D. dissertation at the University of Geneva, 2004), in <http://theory.physics.unige.ch/~trotta>.
- [52] J.M. Bardeen, *Phys. Rev. D* **22**, 1882 (1980); H. Kodama and M. Sasaki, *Prog. Theor. Phys. Suppl.* **78**, 1 (1984); V.F. Mukhanov, H.A. Feldman and R.H. Brandenberger, *Phys. Rep.* **215**, 203 (1992); R. Durrer, *Fund. Cos. Phys.* **15**, 209 (1994) [astro-ph/9311041].
- [53] J.M. Bardeen, P.J. Steinhardt and M.S. Turner, *Phys. Rev. D* **28**, 679 (1983); J. Martin and D.J. Schwarz, *ibid.* **57**, 3302 (1998); D. Wands, K.A. Malik, D.H. Lyth and A.R. Liddle, *ibid.* **62**, 043527 (2000).
- [54] M. Kawasaki and T. Moroi, *Prog. Theor. Phys.* **93**, 879 (1995).
- [55] M.S. Turner, *Phys. Rev. D* **33**, 889 (1986).
- [56] W.L. Freedman *et al.*, *Astrophys. J.* **553**, 47 (2001).
- [57] E.J. Copeland, I.J. Grivell and A.R. Liddle, astro-ph/9712028.
- [58] M. Tegmark and A.J.S. Hamilton, astro-ph/9702019.
- [59] B. Ananthanarayan, Q. Shafi and X.M. Wang, *Phys. Rev. D* **50**, 5980 (1994); M.E. Gomez, G. Lazarides and C. Pallis, *ibid.* **61**, 123512 (2000).
- [60] B. Ananthanarayan, G. Lazarides and Q. Shafi, *Phys. Rev. D* **44**, 1613 (1991); *Phys. Lett. B* **300**, 245 (1993).
- [61] P. de Bernardis *et al.*, *Astrophys. J.* **564**, 559 (2002).
- [62] R. Durrer, B. Novosyadlyj and S. Apunevych, *Astrophys. J.* **583**, 33 (2003).
- [63] <http://cosmologist.info/cosmomc/>.
- [64] A. Lewis and S. Bridle, *Phys. Rev. D* **66**, 103511 (2002).
- [65] J. Väliiviita and V. Muhonen, *Phys. Rev. Lett.* **91**, 131302 (2003).
- [66] R. Bowen, S.H. Hansen, A. Melchiorri, J. Silk and R. Trotta, *Mon. Not. Roy. Astron. Soc.* **334**, 760 (2002); P. Crotty, J. Lesgourgues and S. Pastor, *Phys. Rev. D* **67**, 123005 (2003); E. Pierpaoli, *Mon. Not. Roy. Astron. Soc.* **342**, L63 (2003); S. Hannestad, *J. Cosmol. Astropart. Phys.* **05**, 004 (2003).
- [67] L. Verde *et al.*, *Astrophys. J. Suppl.* **148**, 195 (2003).
- [68] A. Gelman and D. Rubin, *Statist. Sci.* **7**, 457 (1992).
- [69] D.J. MacKay, *Information theory, inference, and learning algorithms* (Cambridge University Press, Cambridge, U.K., 2003).
- [70] G.E. Box and G.C. Tiao, *Bayesian inference in statistical analysis*, Addison-Wesley series in behavioral science: quantitative methods (Addison-Wesley, Reading, Massachusetts, U.S.A., 1973).
- [71] S. Burles, K.M. Nollett and M.S. Turner, *Phys. Rev. D* **63**, 063512 (2001).
- [72] E. Komatsu *et al.*, *Astrophys. J. Suppl.* **148**, 119 (2003).
- [73] D.H. Lyth, *Phys. Rev. D* **45**, 3394 (1992).
- [74] D.V. Lindley, *Biometrika* **44**, 187 (1957); M.S. Bartlett, *ibid.* **44**, 533 (1957).
- [75] R.E. Kass and A.E. Raftery, *J. Amer. Statist. Assoc.* **90**, 773 (1995).
- [76] T.J. DiCiccio, R.E. Kass, A.E. Raftery and L. Wasserman, *J. Amer. Statist. Assoc.* **92**, 903 (1997).